

RESEARCH ARTICLE

Paleohistology of *Caraguatypotherium munozi* (Mammalia, Notoungulata, Mesotheriidae) from the early late Miocene of northern Chile: A preliminary ontogenetic approach

Jorge Campos-Medina  ^{1,2,3*}, Germán Montoya-Sanhueza  ^{4*}, Karen Moreno  ^{1*}, Enrique Bostelmann Torrealba  ^{1,5,6}, Marcelo García ⁷

1 Instituto de Ciencias de la Tierra, Facultad de Ciencias, Universidad Austral de Chile, Valdivia, Región de Los Ríos, Chile, **2** Centro de Estudios Avanzados en Zonas Áridas (CEAZA), Coquimbo, Chile, **3** THERIUM SPA, Paleontología y Patrimonio, Curicó, Región del Maule, **4** Department of Zoology, Faculty of Science, University of South Bohemia, České Budějovice, Czech Republic, **5** Doctorado en Ciencias Mención Ecología y Evolución, Universidad Austral de Chile, Valdivia, Región de Los Ríos, Chile, **6** Museo Regional de Aysén, Coyhaique, Región de Aysén, **7** Departamento de Geología, Universidad de Chile, Santiago, Chile

* jorge.camposmedina@gmail.com (JCM); karenmoreno@uach.cl (KM); g.montoya.sanhueza@gmail.com (GMS)



OPEN ACCESS

Citation: Campos-Medina J, Montoya-Sanhueza G, Moreno K, Bostelmann Torrealba E, García M (2023) Paleohistology of *Caraguatypotherium munozi* (Mammalia, Notoungulata, Mesotheriidae) from the early late Miocene of northern Chile: A preliminary ontogenetic approach. PLoS ONE 18(3): e0273127. <https://doi.org/10.1371/journal.pone.0273127>

Editor: Michael Schubert, Laboratoire de Biologie du Développement de Villefranche-sur-Mer, FRANCE

Received: August 1, 2022

Accepted: February 24, 2023

Published: March 16, 2023

Copyright: © 2023 Campos-Medina et al. This is an open access article distributed under the terms of the [Creative Commons Attribution License](https://creativecommons.org/licenses/by/4.0/), which permits unrestricted use, distribution, and reproduction in any medium, provided the original author and source are credited.

Data Availability Statement: All relevant data are within the paper and supplementary figures.

Funding: KM received funding from 2015 to 2018 for the present research: FONDECYT regular 1150879, Agencia Nacional de Investigación y Desarrollo, <https://www.anid.cl/>. JC-M received funding from FONDART 403858, Fondo Nacional de Desarrollo Cultural y las Artes, <https://www.>

Abstract

The Miocene Caragua fossil fauna in northern Chile contains a considerable number (7) of articulated partial skeletons tentatively assigned to *Caraguatypotherium munozi* (Notoungulata, Mesotheriidae), which presents up to 40% body size difference. Since either inter- and intra-specific wide size range has been observed in the Mesotheriidae family in general, we wanted explore the ontogenetic stage signature of the sample, by carrying out the first comprehensive paleohistological description of the appendicular system in Notoungulata. Results show that: 1) they can be classified as subadults and adults, based on the presence of bone tissues typical of ceased somatic growth; 2) there is a notorious inter-skeletal variation on bone growth rates (skeletal modularity), particularly, the humerus showed a slower diameter growth and less remodelling than the femur, resulting as a better element for ontogenetic analyses; 3) marked cyclical growth is observed, characterised by fast early ontogenetic continuous growth, and subsequent fast/slow stratified bone tissue layering. In general, such growth pattern suggests that *C. munozi* had a similar ontogenetic growth process as other modern mammals, that it should also be influenced by other sex-related, ecological and environmental factors. Likely related to the presence of rapid climatic variations, due to orogenic uplift and concomitant re-organization of the drainage processes along the western tectonic front of the Central Andes at that time.

Introduction

During the Cenozoic, the South American native ungulates (SANUs) represented a particular and diverse group of phylogenetically related clades, presently grouped in the orders

fondosdecultura.cl/ The funders had no role in study design, data collection and analysis, decision to publish, or preparation of the manuscript.

Competing interests: The authors have declared that no competing interests exist.

Abbreviations: CTES-PZ, Corrientes-Paleozoología; HS, Histology; MD-FM, Museo Municipal de Ciencias Naturales “Carlos Darwin”, Punta Alta (Buenos Aires Province); MHNSR-PV, Museo de Historia Natural de San Rafael, Vertebrate Paleontology Collection, San Rafael, Mendoza, Argentina; MNHN, Museum national d’Histoire naturelle, Paris, France; MPEF-PV, Museo Paleontológico Egidio Feruglio- Paleontología de Vertebrados, Trelew, Chubut, Argentina; UACH, Universidad Austral de Chile; XX, Type of bone element (e.g., HI: Left humerus; HD: Right humerus; UD: Right ulna; MTCl: Left metacarpal; PFI: 1st left phalange; Fl: Left femur; FD: Right femur; TI: Left tibia; MTSI: Left metatarsal; PFD: 1st right phalange); XX, Year of field work; Y, Number of sample elements; YPM, Yale Peabody Museum of Natural History, New Haven, Connecticut, USA Identification of individuals: HUAYXX-YY: HUAY: Huaylas; YY, Item number collected. Identification of histological specimens: GEOUACH.HS.XX. Y: GEO: Geology department.

Xenungulata, Pyrotheria, Astrapotheria, Notoungulata and Litopterna, plus few endemic, early Paleogene “condylarthra” [1–3]. These extinct mammals exhibited one of the most divergent variety of body sizes and morphological adaptations, including fully cursorial locomotion in the medium sized Proterotheriidae [4], mass graviportal standing in gigantic toxodontids, astrapotheres, and pyrotheres [5–8], and scansorial, cursorial and semi-fossorial habits in diverse lineages within the small to medium-sized typotheres [9–11]. Studies based on collagen protein chains (proteomics) extracted from Pleistocene fossils (i.e., Toxodontia and Litopterna), have placed SANUs within Laurasiatheria, specifically as a sister group to extant Perissodactyla (e.g. tapirs, horses and rhinoceroses) [12–14]. Nevertheless, recent morphological phylogenetic studies have proposed alternative relationships, identifying them as a non-monophyletic group [4, 8, 15, 16]. In this sense the study of their biology and evolution have represented one of the most challenging tasks for vertebrate palaeontologists since the end of the 19th century [1, 15]. Although some aspects of their paleobiology such as their locomotor modes and general lifestyle have been documented (e.g. [9, 16–18]), other important aspects such as their skeletal growth and development remain largely unknown (but see [19] for cranial features).

Paleohistology is a useful tool for elucidating the growth patterns, life history and physiology of extinct vertebrates [20–25]. It has provided insights on several aspects of the evolutionary biology of extinct mammals including the reconstruction of their growth and development [22, 26–29], adaptations to different lifestyles [27], ecology [22, 29, 30] and physiology [22, 27]. However, the studies on the paleohistology of extinct mammals of South American faunas are still scarce. For example, de Ricqlès *et al.* [31] reviewed the paleohistological collection of Paul Gervais in Paris (Laboratory of Comparative Anatomy of the Museum of Natural History), and briefly described some elements of notoungulates such as an ulna of *Toxodon* sp. (Toxodontidae), and various cross-sections of ulna, molars and incisors initially assigned to Typotherium, and presently recognized as *Mesotherium* sp. [32, 33] (Mesotheriidae, Simpson, 1940). More recently, Tomassini *et al.* [34, 35] analysed the paleohistology of *Paedotherium bonaerense* (Hegetotheriidae) and *Toxodon platensis*, and documented fossil-diagenetic modifications in their bone microstructure. Forasiepi *et al.* [36] and Carrillo and Asher [37] also provided a general paleohistological description of a new toxodontid species (*Nesodon taweretus*), and of an extremely well-preserved skeleton of *Thomashuxleya externa* (Isotemnidae) respectively. Houssaye *et al.* [18] analysed the bone microanatomy of several SANUs including Pyrotheria, Astrapotheria and Notoungulata. The latter authors quantified the relative proportions of compact and trabecular bone regions using CT scans to infer locomotor adaptations, although no paleohistological descriptions were included.

Considering this information, no attempts to assess the growth patterns and development of these extinct mammals throughout bone paleohistology have been done. Clearly, the study of ontogenetic series including several individuals, more taxonomically restricted taxa, as well as the incorporation of different bone elements, would largely improve our knowledge on the paleobiology of these extinct animals.

Mesotheriids and specifically the subfamily Mesotheriinae are one of the most late diverging groups within the suborder Typotheria, being common faunal elements during the Neogene at mid-latitude Andean localities, and lowland Pampean ecosystems (for a detailed account of their diversity, evolution, taxonomy and distribution see [38–45], until their final disappearance during the middle Pleistocene (Chibanian) [44, 45]. Despite this, many aspects of their biology and paleoecology are largely unknown. Particularly interesting is the presence of large cranio-dental size differences within ontogenetic series in various Mesotheriidae [33, 40, 46].

The present study describes in detail the long bone paleohistology of several individuals assigned to *C. munozii*, based on their restricted stratigraphical and local distribution at the Miocene Copaquilla basin, northern Chile. Because the material collected exhibits clear differences in body size among individuals (Table 1) it becomes fundamental to uncover the real nature of such variation, whether resulting from ontogenetic differences or the presence of

Table 1. Bone measurements (cm) of seven individuals of *Caraguatypotherium munozii* from Huaylas formation.

INDIVIDUALS and code	Bone element	Total length	Inferred midshaft length (craniodistal, antero/posterior)	Anteroposterior diameter at the midshaft (approx. 50% of total length)	Lateromedial diameter at the midshaft (approx. 50% of total length)
Individual 1: HUAY15-100					
GEOUACH.HS.HI.1	Left humerus	20.5	10.23	2.75	2.29
GEOUACH.HS.MTC.2	Left Mc III	7.24	3.62	0.85	1
GEOUACH.HS.PFI.1	1 st left phalange	2.79	1.395	0.62	1.02
Individual 2: HUAY15-200					
GEOUACH.HS.HD.1	Right humerus*	19.53	9.5	2.74	1.57
GEOUACH.HS.UD.1	Right ulna**	23.2	11.6	2.32	1.1
GEOUACH.HS.PFD.1	1 st right phalange	2.55	1.2	0.64	0.84
GEOUACH.HS.FI.1	Left femur***	20.44	10.5	1.4	2.25
Individual 3: HUAY17-05					
GEOUACH.HI.2	Left humerus*	12.4	6.2	1.64	1.24
Individual 4: HUAY16-100					
GEOUACH.HS.TI.1	Left tibia*	13.3	6.65	1.55	1.09
GEOUACH.HS.MTSI.1	Left Mt II	4.48	2.42	0.57	0.81
Individual 5: HUAY15-084					
GEOUACH.HS.FI.2	Left femur***	16.4	8.2	1.46	1.81
GEOUACH.HS.TI.2	Left tibia*	12.41	6.2	1.4	1.04
Individual 6: HUAY15-027					
GEOUACH.HS.TI.3	Left tibia***	17.4	8.7	1.7	1.21
Individual 7: HUAY17-02					
GEOUACH.HS.FD.1	Right femur**	23.3	11.65	11	-

Total bone length and corresponding midshaft was inferred in the material were the:

*proximal epiphysis is missing,

**distal epiphysis is missing; or

***both epiphyses are missing

<https://doi.org/10.1371/journal.pone.0273127.t001>

multiple taxa in the region. Based on this observation, we hypothesise that the smaller individuals represent young individuals of *C. munozii*, and therefore their bones will exhibit typical osteohistological features of mammalian juveniles/subadults, such as disorganised and relatively fast deposition of bone tissues, highly vascularized cortices and comparatively lower levels of secondary bone remodelling. In contrast, larger individuals will reflect more advanced ontogenetic stages, with typical osteohistological features of adult mammals, such as slowly deposited bone tissues, increased bone remodelling, and evidence of growth marks. This study discusses the potential factors explaining the morphological variation of the remains assigned to *C. munozii*, in terms of ontogeny, intraspecific variation, and interskeletal variation, thus providing a basis for future palaeohistological comparisons of Mesotheriidae and other Notoungulates.

Geological context

The Caragua vertebrate assemblage was collected from the Huaylas Formation [47–49], exposed in the eastern Precordillera of Arica at ~18.5°S, currently at 2,900–3100 m.a.s.l. (Fig 1). To the west of Caragua, the Precordillera consists of the late Miocene Oxaya Anticline, which is a large, west-vergent, gentle fold; to the east, the Western Cordillera is formed by a Miocene fold-and-fault belt involving the Precambrian-Paleozoic metamorphic basement [47, 49–51]. The Huaylas Formation consists of polymictic sandstones and semi-consolidate

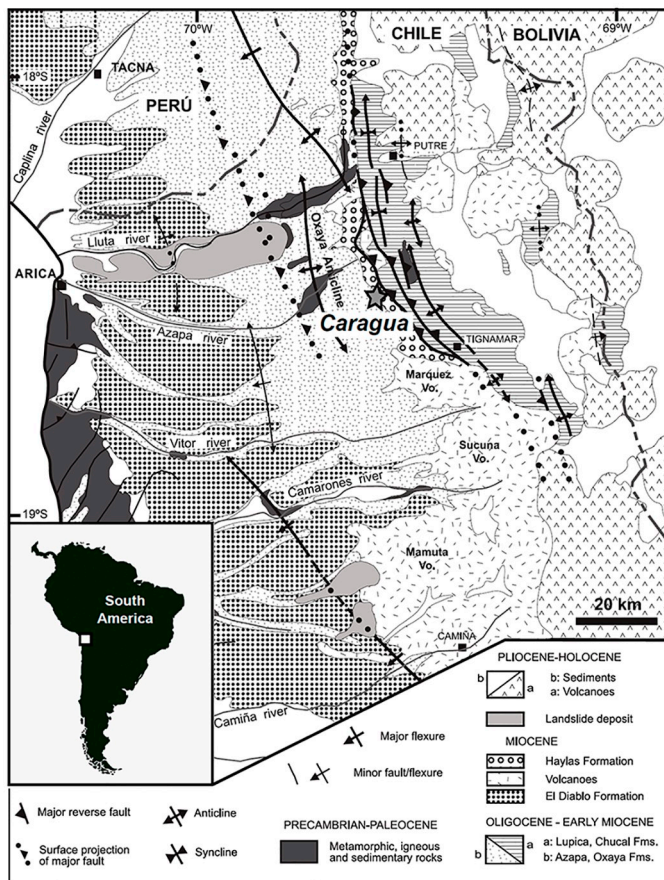


Fig 1. Geographic and geological map. Geographic and geological setting of the Caragua fossil locality (star), in northern Chile, showing the main litho-stratigraphic units and structural features; adapted from García et al. [48].

<https://doi.org/10.1371/journal.pone.0273127.g001>

gravels, which were deposited predominantly in a fluvial environment and subordinately in an alluvial setting. K-Ar and Ar/Ar dates of volcanic rocks indicate that the fossiliferous beds were deposited between 11.7 ± 0.7 Ma and 10.7 ± 0.3 Ma, early late Miocene [47–49] (Tortonian, [52]).

The fluvial-alluvial environment of the Huaylas Formation rocks and the presence of middle Miocene episodic drainage systems reflecting a semi-arid climate contrasts with the modern hyper-arid climate conditions present in the region [48, 53, 89]. This changing environmental setting represents a unique opportunity to assess the role of major geomorphological processes on the associated fauna.

Materials and methods

Material of *Caraguatypotherium munozii*

The Caragua fossil fauna include several mammals [54–58], in which *C. munozii* is the most abundant [58] and represented by a diversity of cranial and postcranial elements with variable degrees of preservation. Multiple appendicular elements of seven individuals were analysed. Taxonomical assignation to *C. munozii* was based on anatomical similarities and proportions, dental homologies, and their restricted stratigraphical and localised spatial distribution in the outcrops. Three individuals include cranial and dental elements (HUAY15-100; HUAY15-200; HUAY17-05). The fossil materials were collected during a series of field campaigns in the Huaylas Formation between 2015 and 2017 (List of materials: Table 1). The materials are currently deposited at the Instituto de Ciencias de la Tierra, Universidad Austral de Chile.

Postcranial bone morphology and external measurements

The bone material was measured either directly with a digital calliper or using a software of image processing, ImageJ [59], after reconstruction. Because several bones were fragmented or lacked one or both epiphyses, full reconstructions of the bone material was based on the comparison with more complete skeletons of closely related mesotheriines (e.g. *Plesiotypotherium* [58, 60, 61]). This allowed us to ensure that our histological samples are come from the midshaft. Three linear measurements of the long bones were obtained: the total length of the bone, measured from the proximal articular surface to the distal articular surface; and the anteroposterior and mediolateral diameters of the diaphysis, both taken approximately at the midshaft (around 50% from the proximal articular surface) (Table 1). We also assessed the gross skeletal maturity of each element (when possible) by classifying the degree of epiphyseal fusion (adult stage), as fused and not fused (juvenile stage) (Table 1) given the highly conservative shape of the appendicular skeleton in mesotheriids [9, 61]. Virtual completion of bone elements from scaled images was performed using Adobe Photoshop CC and Adobe Illustrator CC (Adobe Systems Inc.).

High quality photographs of each bone in anterior, posterior, medial, and lateral views were taken using a DSLR camera Canon EOS Rebel T6. Digital replicas of the fossils were created with a Go!SCAN 3D.20 scanner using the VXElements software (Creaform Inc.). All procedures were carried out at the Laboratorio de Observación y Documentación, at the Instituto de Ciencias de la Tierra (Universidad Austral de Chile, Valdivia). Additionally, silicone replicas were created following the methodology used by Reuil and Muzzopappa [62], at the Laboratorio de Paleontología (Universidad Austral de Chile, LabPALEO-UACH).

Paleohistological procedures

A total of fourteen paleohistological cross-sections were obtained from forelimbs and hindlimbs of seven individuals (Table 1). Thin sections were prepared following standard

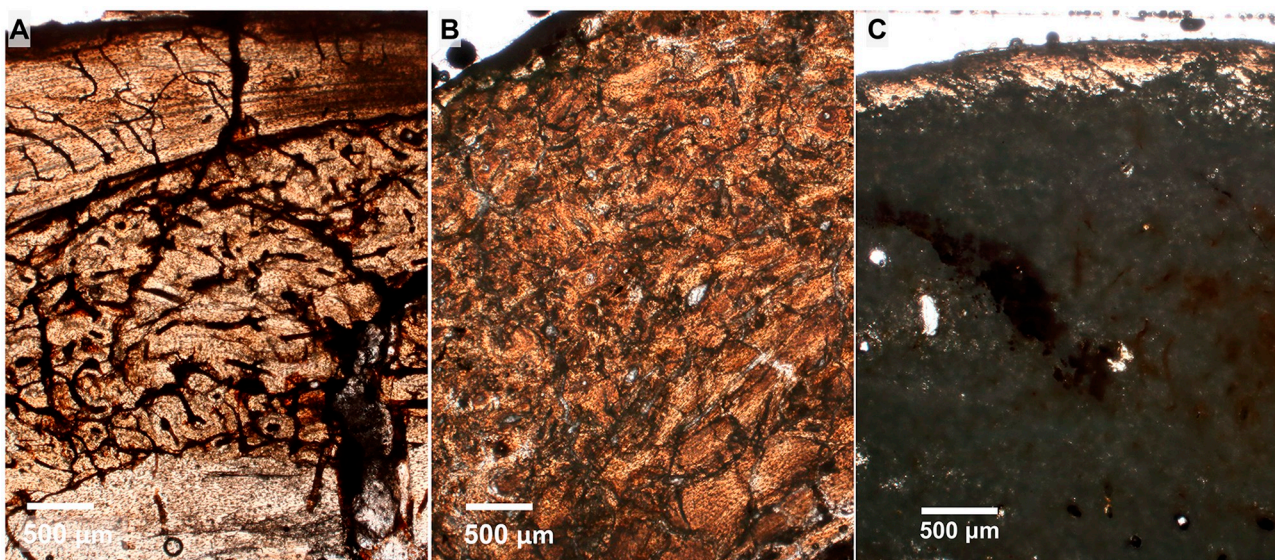


Fig 2. Degree of preservation in specimens of *Caraguatypotherium munozi* following the methodology used by Hollund et al. [69]. (A) State 1, well preserved (GEOUACH.HS.HD.1); (B) State 2, intermediate preservation (GEOUACH.HS.FD.1); (C) State 3, poor preservation (GEOUACH.HS.FI.1).

<https://doi.org/10.1371/journal.pone.0273127.g002>

histological protocols defined by Chinsamy and Raath [63]. The preparation and housing of specimens corresponds to LabPALEO-UACH. Cross-sections were performed at the midshaft of the diaphysis, i.e., ~50% from the proximal articular surface. This region of the bone is usually not excessively remodelled or resorbed in mammals as compared to the more proximal and distal regions of the bone, thus preserving a relatively complete sequence of the animal growth (i.e. [21, 27, 30, 64–68]).

Because of the varying degrees of preservation of the bone material, we qualitatively classified them into three categories based on the degree of histological preservation [69]. These categories are based on the capacity to observe histological structures under the petrographic microscope (Fig 2): State 1 (well preserved), characterised by a relatively complete integrity of the bone microstructure; State 2 (intermediate preservation), refers to the partial preservation of histological characteristics in the section; and State 3 (poor preservation), with null or very scant observation of histological features in the section.

Paleohistological nomenclature

A detailed qualitative description of the anterior, posterior, lateral and medial sides of the cross-section was carried out for each bone element. For this, the bone cortex was arbitrarily divided into three regions: endocortical, intracortical and pericortical (Fig 3) [68].

The description of the bone microstructure was carried out using an optic petrographic microscope Zeiss Axio Scope A1 and polarised light with a lambda filter to observe the direction of collagen fibres. Histological descriptions of the bone tissues were made following the classical studies on vertebrate osteohistology (Enlow [70], Francillon-Vieillot *et al.* [71] and de Ricqlès *et al.* [72]). We identified the shape and relative size of the osteocyte lacunae, the orientation of the mineralized collagen fibres, and the predominant matrix type of the cortex and its vascularization.

Types of bone matrix according distinct ontogenetical stages.

1. Woven (WB) and fibrolamellar bone (FLB): composed of collagen fibres of multidirectional cortical distribution, monorefringent under the microscope with polarised light

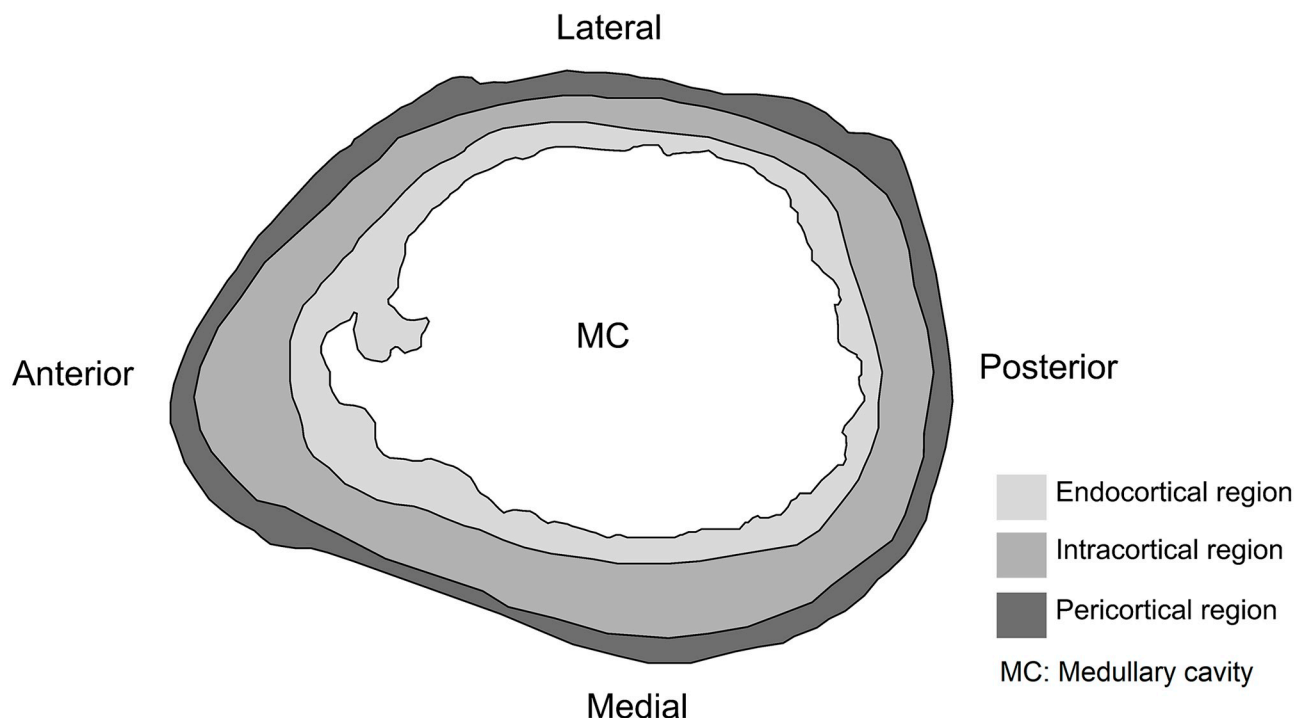


Fig 3. Right humerus cross-section diagram. Divisions of bone cortex used to describe paleohistological samples in *Caraguatypotherium munizi*.

<https://doi.org/10.1371/journal.pone.0273127.g003>

(independent of the longitudinal or transverse direction of the cut). Typically, this type of bone tissue presents randomly distributed and globular osteocyte lacunae and is usually associated with a high rate of osteogenesis and high vascularization. If primary osteons are present within the WB, having a more anisotropic structure, it is termed as FLB.

2. Compacted coarse cancellous bone (CCCB): type of bone found primarily in the epiphyseal plates and that through modelling can be encountered in the middle part of the diaphysis [68]. In young individuals, the ends of their long bones comprise endochondral cancellous bone, but as the animal matures the "ends" become incorporated into the bone wall of the older individual. In the process, the cancellous bone becomes compacted with lamellar bone deposits which fill in the cancellous spaces. The bone tissue characteristically has a swirled, convoluted appearance.
3. Parallel-fibered bone (PFB): Composed of tightly packed collagen fibres, usually with the same orientation, mono or birefringent under polarised light microscope (depending on the transverse or longitudinal direction of the cut). It presents flattened and relatively organised osteocyte lacunae. This type of bone is usually associated with a lower osteogenesis rate as compared with WB.
4. Lamellar bone (LB): It presents the higher degree of organisation of collagen fibres and is composed of successive thin layers called lamellae that correspond to tightly packed collagen fibres. The visualisation under polarised light microscope is variable (mono or birefringent). Each lamella usually contains rows of flattened osteocyte lacunae. This type of bone tissue is usually associated with a lower rate of osteogenesis and poor vascularization as compared to PFB.

Ontogenetic paleohistology. In general, the postnatal morphogenesis of long bones of mammals follows a relatively conserved pattern of bone matrix formation, from more rapidly deposited bone tissues (e.g., WB) to slowly deposited bone tissues (e.g., LB) (see [65]), and references therein). This generalised sequence of bone tissue formation has been useful to identify different ontogenetic stages in extinct mammalian species [21, 73]. Thus, predominantly more disorganised bone matrices with large and globular osteocyte lacunae and lacking any obvious organisation of their collagen fibres (e.g. WB) would account for a relatively less mature bone and therefore to earlier stages of development (e.g. juvenile individuals). In contrast, a more mature bone would display a higher degree of organisation of its collagen fibres and bone matrix, with usually smaller osteocyte lacunae of fusiform shape (e.g., LB), which is typical of more advanced stages of somatic maturity (i.e. adult individuals).

It has been reported that the cease of somatic growth in some vertebrates is characterised by the formation of a layer of periosteal lamellar bone (PLB), generally called external fundamental system (EFS) by some authors [27] or outer circumferential layer (OCL) by others [70]. This is a clear indicator of low rates of bone deposition, characteristic of many vertebrates including mammals in advanced stages of somatic maturity (e.g. [21, 27, 68]).

Overall, to describe bone growth, we make emphasis on describing the processes of bone modelling finally observable at the midshaft, which involves the formation and resorption of bone tissues in a coupled or uncoupled mechanism acting in different bone surfaces [68]. This process is responsible for the main longitudinal and diametrical growth of the bone, thus resulting in both shape and size changes during ontogeny [68]. Bone modelling is synonymous to Enlow's [70] term "growth remodelling". We also describe bone remodelling, which refers to the formation of Haversian systems, sometimes resulting in dense aggregations of secondary osteons covering the bone surface, termed dense Haversian bone [70].

It is important to consider that the above definitions are not definitive, mainly because the bone matrix composition of a single element and/or one individual can vary considerably in its arrangement (e.g. [64, 65, 74, 75]). For this reason, to properly determine ontogenetic stages in individuals, it is necessary to consider the assessment of complete transversal sections of different bone, and when possible, include multiple elements to assess inter-skeletal variation. Other histological features associated with ontogeny in mammals include the development of secondary osteons and its extension over the bone surface (bone remodelling and development of Haversian bone). Considering that each individual of *C. munozi* possess more than one bone element, we summarize the ontogenetic inferences obtained from the paleohistological description for each individual. The final ontogenetic stage is defined by the elements exhibiting the most active bone modelling activity, and are described from the most proximal to the most distal elements.

Results

Distinct bone tissue matrices were present in the appendicular skeleton of *C. munozi*: fibrolamellar bone (FLB), compacted coarse cancellous bone (CCCB) parallel fibered bone (PFB), lamellar bone (LB), and Haversian bone (HB). All the sections showed varying amounts of some of these tissues. Simple vascular canals (VC), radial vascular canals (RVC), reticular vascular canals (REVC), plexiform vascular canals (PVC), canals of the nutrient arteries (CNA), resorption cavities (RC), as well as primary (PO) and secondary osteons (SO), were also found in the sections (Fig 4). General descriptions of these bone tissue types and its distribution within the cross-sections is presented below.



Fig 4. Bone tissue types observed in *Caraguatypotherium munozii*. (A) Fibrolamellar bone (FLB);(GEOUACH.HS.UD.1); (B) Compacted coarse cancellous bone (CCCB) and reticular vascular canals (REVC);(GEOUACH.HS.UD.1); (C) Parallel fibered bone (PFB), radial vascular canals (RVC) and compacted coarse cancellous bone (CCCB);(GEOUACH.HS.PFD.1); (D) Lamellar bone (LB) and secondary osteons (SO);(GEOUACH.HS.TI.2); (E) Haversian bone (HB);(GEOUACH.HS.FI.2); (F) Plexiform vascular canal (PVC) and parallel fibered bone (PFB);(GEOUACH.HS.UD.1); (G) Primary osteon (PO), Parallel fibered bone (PFB), Canal of the nutrient artery (CNA) and Compacted coarse cancellous bone (CCCB);(GEOUACH.HS.PFD.1).

<https://doi.org/10.1371/journal.pone.0273127.g004>

Histodiversity and bone growth

Humerus. *Bone microanatomy.* Three distinct humeri were analysed for distinct individuals: Individual 1, individual 2 and individual 3 (Table 1, Fig 5A–5C). The cross-section is ellipsoidal, elongated in antero-posterior direction, probably because of the development of both the deltopectoral crest in the anterior side and the supracondylar crest in the posterolateral side of the diaphysis [61]. The three individuals exhibited an open medullary cavity with fragmented remains of trabecular organisation, mostly localised in the anterior side.

Bone microstructure. The endocortical region is composed of bands of LB and PFB of different thicknesses that surround the medullary cavity (Fig 5D, 5G, 5H and 5K). The vascularization of the endocortical region is mostly of radial type.

The intracortical region is highly variable in bone tissue composition. The intracortical region of the humerus of individual 3 is almost completely composed of CCCB (Fig 5K), and contrasts with the other individuals in that they exhibit both CCCB and FLB in the anterior side (Fig 5I). The medial and lateral sides are composed of FLB, with development of SO in the individual 1 (Fig 5D and 5E), while the posterior region exhibited intercalations of PFB and LB, with presence of PO and SO (Fig 5F and 5H). Conspicuous vascularization is observed in the anterior side, corresponding to REVC and RVC (Fig 5I).

The pericortical region of the humeri exhibited both PFB and LB (Fig 5G, 5K and 5L). These tissues surround the whole bone section, and are thinner or absent in the anterior side, where CCCB and FLB predominate. The posterior side of the humeri presented relatively

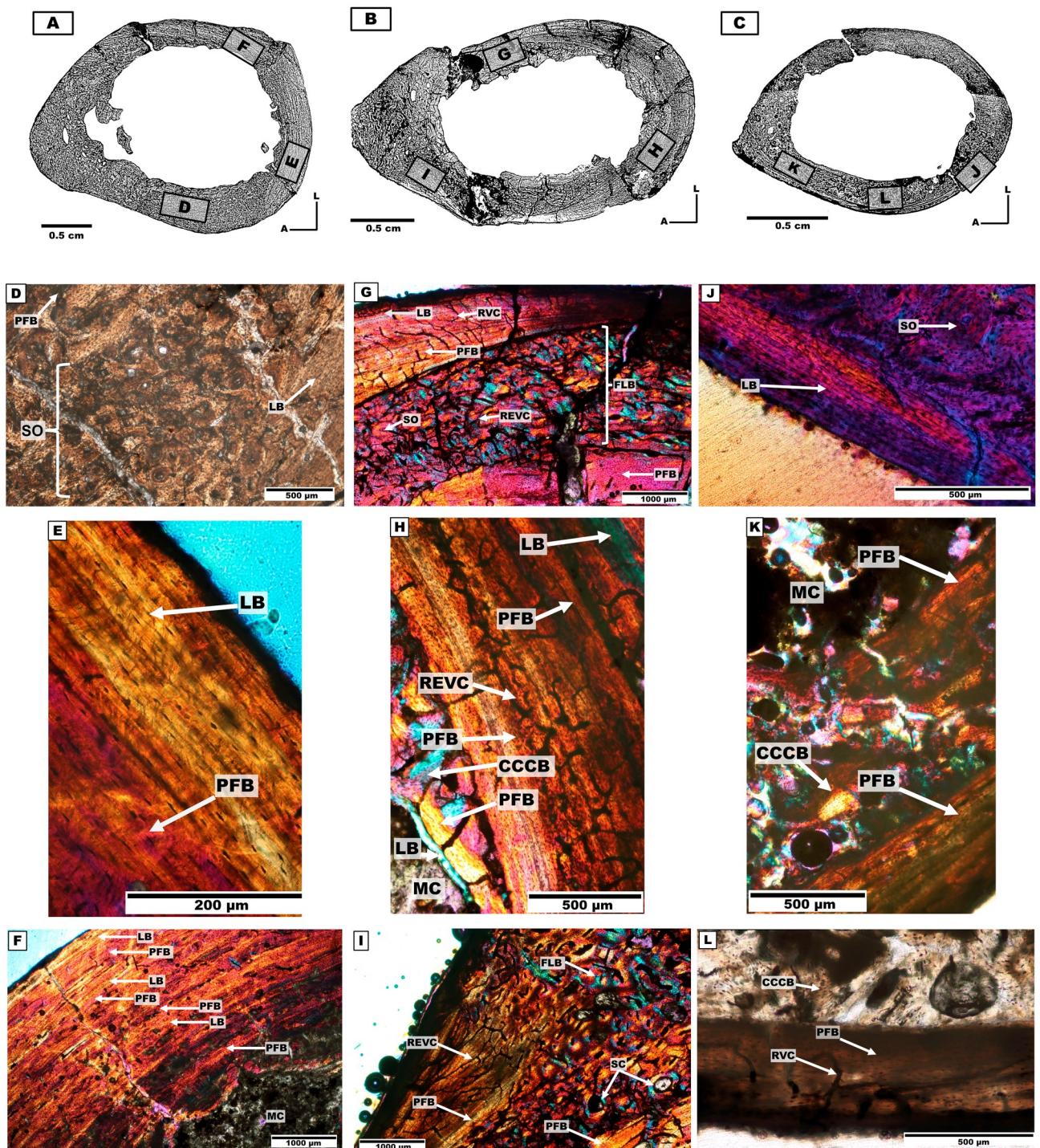


Fig 5. Distinct humerus cross-sections of the mesotheriine notoungulate *Caraguatypotherium munozi* from the middle Miocene of Caragua, Huaylas formation. (A) Humerus cross-section for individual 1 (GEOUACH.HS.HI.1); (B) Humerus cross-section for individual 2 (GEOUACH.HS.HD.1); (C) Humerus cross-section for individual 3 (GEOUACH.HI.1); (D) PFB in the endocortical region, SO in the intracortical region, LB in the pericortical region (GEOUACH.HS.HI.1); (E) PFB in the intracortical region and LB in the pericortical region (GEOUACH.HS.HI.1); (F) Intercalation of LB and PFB in the posterior area (GEOUACH.HS.HI.1); (G) Endocortical and pericortical region presence of LB and PFB, intracortical region presence FLB and SO (GEOUACH.HS.HD.1); (H) LB in the endocortical region, CCCB, PFB and LB in the intracortical region (GEOUACH.HS.HD.1); (I) Anterior area, FLB in the intracortical region, in the lateral area PFB and abundant vascularity (GEOUACH.HS.HD.1); (J) SO in the intracortical region, LB in the pericortical region (GEOUACH.HI.2); (K) PFB in the endocortical and pericortical region, CCCB in the intracortical region (GEOUACH.HI.2); (L) PFB in the pericortical region, RVC in this region open, in the intracortical region CCCB (GEOUACH.HI.2). For abbreviations refer to Fig 4.

<https://doi.org/10.1371/journal.pone.0273127.g005>

thicker bands of well-defined LB as compared to the rest of the cross-section (Fig 5F and 5H), and the three humeri of individuals 1–3 present EPS. The pericortical vascularization of the humerus of individuals 1 and 2 is minimal or absent in comparison to the humerus of individual 3, which exhibited mostly RVC and REVC, sometimes opened to the external surface (Fig 5L), thus indicating active osteogenesis.

Ulna. *Bone microanatomy.* The ulna of the individual 2 was analysed (Table 1, Fig 6A). It is clearly elliptical, with the antero-posterior axis of the section being much longer than the medio-lateral axis. There is a conspicuous medullary cavity, also of ellipsoidal shape, with presence of trabecular bone.

Bone microstructure. The endocortical region exhibits CCCB in the posterior area, which decreases its thickness towards the lateral and posterior side. Presence of REVC is identified. In the lateral area, PFB and the presence of REVC are observed. The medial area presents PFB with PVC (Fig 6C). In the anterior area, CCCB and FLB are identified with the presence of SO and REVC (Fig 6D).

In the intracortical region, the posterior area shows CCCB, the medial area presents FLB, and REVC are observed around the entire region (Fig 6E). The lateral area presents CCCB and PFB with REVC. The medial area presents PFB with the presence of PVC. The anterior area presents FLB with the presence of SO, towards the extreme edge in this area RVC is identified.

The pericortical region presents LB forming EFS around the entire section, although composed of bands of different thicknesses. Towards the middle of the posterior area, PFB with SO and LB is observed (Fig 6E).

Metacarpal III. *Bone microanatomy.* The metacarpal III of the individual 1 was analysed (Table 1, Fig 6B). The cross-section is triangular with rounded borders.

Bone microstructure. The endocortical region is characterised by the presence of PFB around the medullary cavity and RVC (Fig 6F). Resorption cavities are present in the posterior side.

The intracortical region is defined by presenting FLB with randomly distributed SO. These are more abundant in the posterior side compared to the rest of the section. PO are observed in the posterior, lateral and medial sides. The intracortical region also presents VC. The anterior, medial and lateral sides present bands of LB (annuli) and PFB with SO (Fig 6G). The bands are thicker in the lateral and posteromedial sides compared to the rest of the section (Fig 6B, 6F and 6G).

The pericortical region presents bands of LB and PFB covering almost the entire external surface of the cross-section, except for a small area of the posterior side where FLB is observed (Fig 6F and 6G).

First phalanges (forelimb). *Bone microanatomy.* Two first phalanges were studied, one from individual 1 and another from individual 2 (Table 1, Fig 7A and 7B). The cross-sections are sub-triangular, and present an open medullary cavity with the same morphology of the cross-section.

Bone microstructure. A conspicuous band of LB and PFB surrounds the entire medullary cavity, which is thicker in the posterior side. RVC are open to the medullary cavity and are more abundant in the posterior side (Fig 7C and 7E). The intracortical region presents FLB and CCCB, and isolated SO (Fig 7D–7F).

The pericortical region shows PFB and LB (Fig 7C and 7E), and RVCs appeared open to the external surface only in the phalange of individual 2 (Fig 7E).

Femur. *Bone microanatomy.* Two femora, of individual 5 and 7 were studied (Table 1, Fig 8A and 8B). The cross-section has a sub-rectangular morphology (mediolaterally elongated), with rounded borders and thick cortical walls. An open and ellipsoidal medullary cavity was present with no trabecular formation.

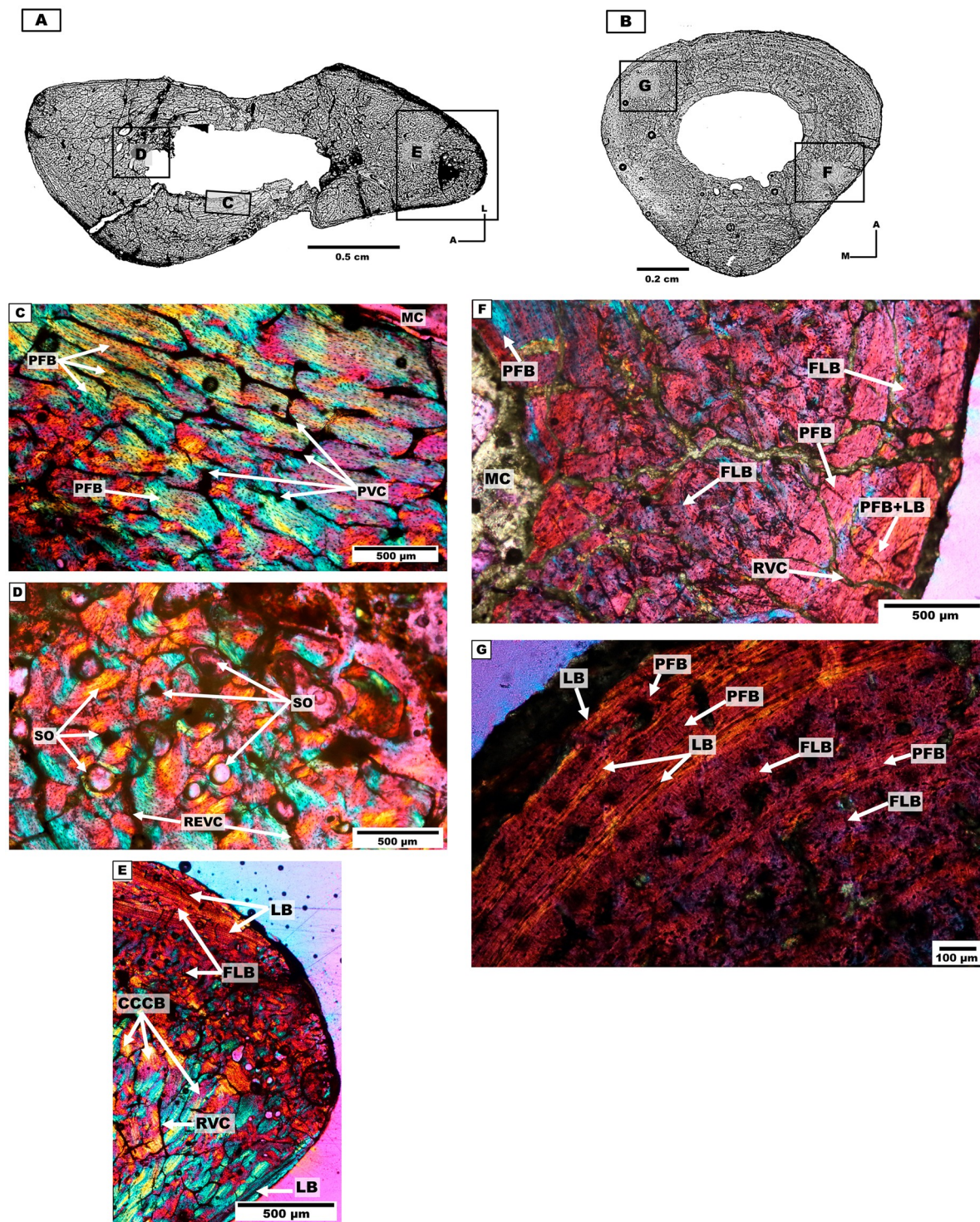


Fig 6. Ulnar and metacarpal III cross-sections of the mesotheriine notoungulate *Caraguatypotherium munozii* from middle Miocene of Caraguá, Huaylas formation. (A) Ulna cross-section for individual 2 (GEOUACH.HS.UD.1); (B) Metacarpal III cross-section for individual 1 (GEOUACH.HS.MTC.2); (C) Intracortical region, presence of PFB with PVC (GEOUACH.HS.UD.1); (D) SO, in the endocortical region (GEOUACH.HS.UD.1); (E) Posterior area of the section, presence of CCCB, LB and PFB are identified. Vascularization dominated by RVC (GEOUACH.HS.UD.1); (F) PFB in the endocortical region, FLB in the intracortical region PFB and LB in the pericortical region GEOUACH.HS.MTC.2); (G) In the intracortical region and pericortical region intercalation of LB with PFB (GEOUACH.HS.MTC.2). For abbreviations refer to Fig 4.

<https://doi.org/10.1371/journal.pone.0273127.g006>

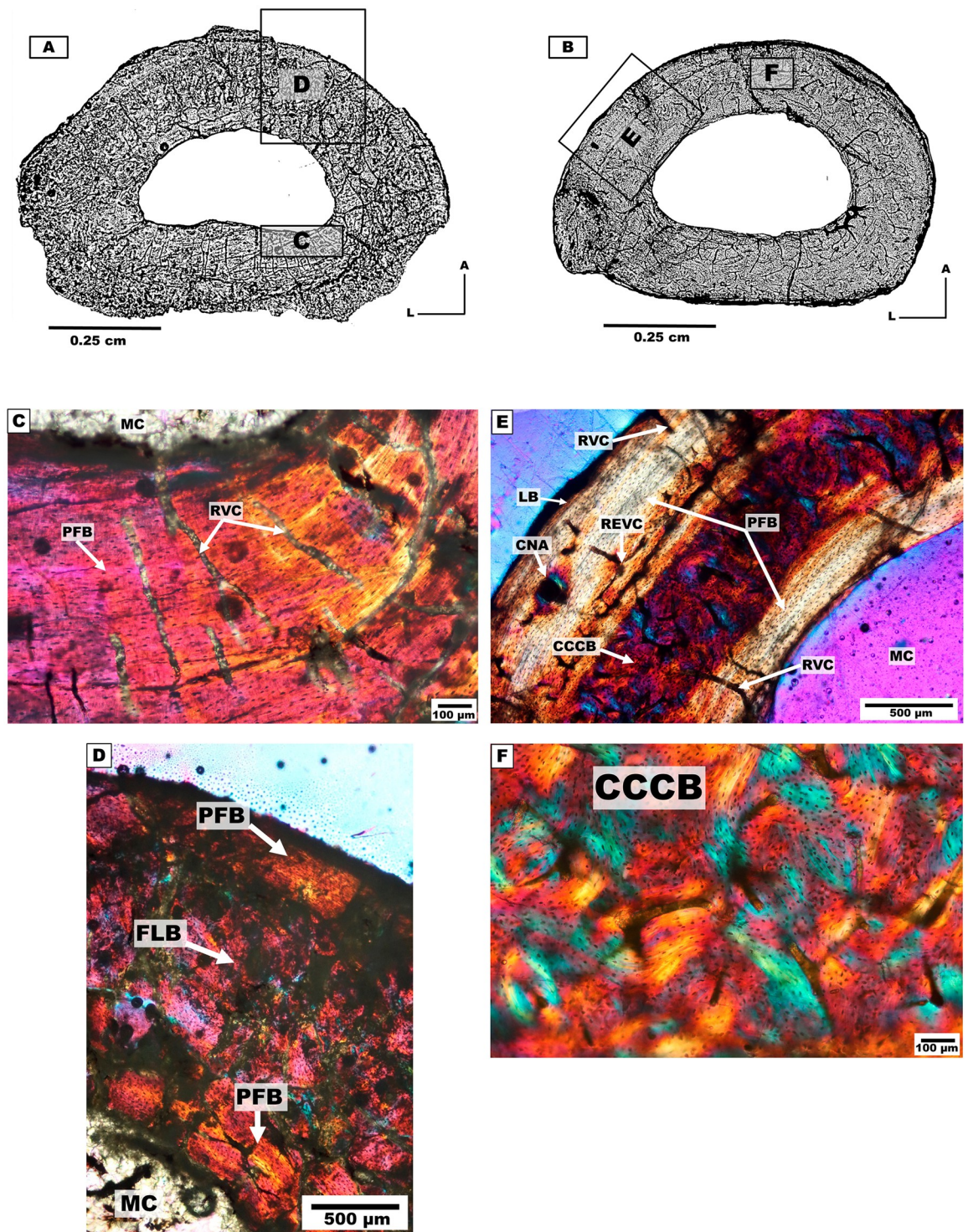


Fig 7. First phalanges cross-sections of the mesotheriine notoungulate *Caraguatypotherium munozi* from middle Miocene of Caragua, Huaylas formation. (A) First phalange cross-section for individual 1 (GEOUACH.HS.PFI.1); (B) First phalange cross section for individual 2 (GEOUACH.HS.PFD.1); (C) Endocortical region presence PFV and RVC can open to the medullary cavity (GEOUACH.HS.PFI.1); (D) FLB in the intracortical region and PFB in the pericortical region (GEOUACH.HS.PFI.1); (E) Diversity of structures in sections, PFB with RVC in the endocortical region, CCCB in the intracortical region, LB and PFB in the pericortical region with presence of RVC and CNA (GEOUACH.HS.PFD.1); (F) CCCB in the intracortical region (GEOUACH.HS.PFD.1). For abbreviations refer to Fig 4.

<https://doi.org/10.1371/journal.pone.0273127.g007>

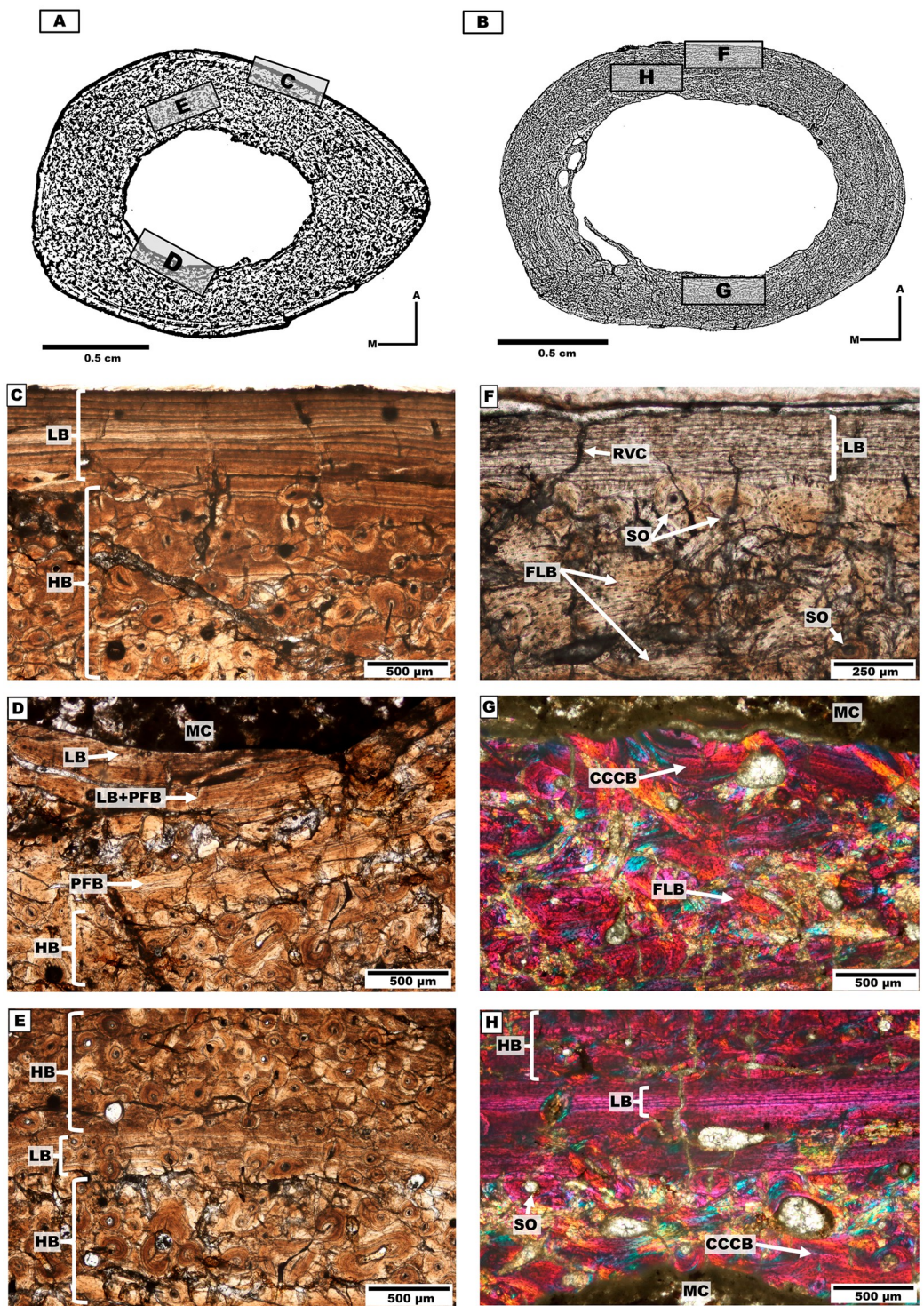


Fig 8. Femurs cross-sections of the mesotheriine notoungulate *Caraguatypotherium munozii* from middle Miocene of Caragua, Huaylas formation. (A) Femora cross-section for individual 5 (GEOUACH.HS.FL.2); (B) Femora cross-section for individual 7 (GEOUACH.HS.FD.1); (C) Pericortical region presence of LB and intracortical region presence of HB (GEOUACH.HS.FL.2); (D) LB and PFB in the Endocortical region (GEOUACH.HS.FL.2); (E) In the centre of intracortical region presence of LB between HB (GEOUACH.HS.FL.2); (F) Pericortical region, presence of LB in the external surface, FLB in the intracortical region and SO (GEOUACH.HS.FD.1); (G) CCCB in the endocortical region and FLB (GEOUACH.HS.FD.1); (H) In the centre of intracortical region presence of LB between HB (GEOUACH.HS.FD.1). For abbreviations refer to Fig 4.

<https://doi.org/10.1371/journal.pone.0273127.g008>

Bone microstructure. The endocortical region in the anterior, lateral and medial areas presents PFB and LB (Fig 8D), while the posterior area presents CCCB and scarce SOs (Fig 8G and 8H).

The intracortical region shows development of HB, although the interstitial primary matrix of FLB was still noticeable (Fig 8E–8H). The anterior region shows LB strongly stratified (Fig 8C and 8H). The intracortical region was almost completely remodelled with HB tissue, and only some RVC were discernible. The pericortical region is stratified showing intercalated bands of LB (Fig 8C and 8F).

Tibia. *Bone microanatomy.* Three tibiae from individuals 4, 5 and 6 were described (Table 1, Fig 9A–9C). The cross-sections have an ellipsoidal shape with sharper pronunciation in the lateral region.

Bone microstructure. The endocortical region shows PFB and LB surrounding the medullary cavity. Open to the medullary cavity appear RVC and sometimes associated with resorption cavities present in the region (Fig 9F, 9G and 9L).

The intracortical region shows a high degree of bone remodelling with formation of HB (Fig 9D–9J), although the interstitial spaces of a primary matrix corresponding to PFB are still observed in some areas (Fig 9J). The pericortical region shows a band of LB (EFS) which is increased in width in the medial side (Fig 9E, 9G, 9K).

Metatarsal II. *Bone microanatomy.* One metatarsal II from individual 4 was analysed (Tables 1–3, Fig 10A). The cross-section is ellipsoidal and contains a rounded medullary cavity with the presence of trabeculae.

Bone microstructure. The endocortical region shows LB surrounding the whole medullary cavity. The posterior, medial and lateral sides present enlarged vascular canals (RVC) under resorption (Fig 10B).

The intracortical region presents FLB with development of SOs in the medial and postero-medial sides, and extending towards the pericortical region. The rest of the section (anterior and lateral sides) did not exhibit considerable remodelling or HB (Fig 10B and 10C).

The pericortical region exhibited LB (EFS) of variable thickness around the bone surface, which is wider in the posterior side and thinner in the lateral side (Fig 10C).

Individual 1 (HUAY15-100). Considering the histological description made for the left humerus (GEOUACH.HS.HI.1; Fig 11A), it is possible to infer a rapid growth (presence of FLB) in the anterior and anterolateral side. Predominance of LB is observed, although the medial side shows clear intracortical remodelling. In the lateral side, FLB is observed in the intracortical region, with some degree of remodelling (SO). EFS is observed in the pericortical region.

In the posterior side, the EFS is extensive, almost covering the entire cortex, with isolated SO.

The sample corresponding to the left metacarpal III (GEOUACH.HS.MTC.1; Fig 11B) allowed identification of FLB tissue in the intracortical region, which is alternated with slow growing bone types in the anterior, lateral and medial sides, thus forming zonal bone. This information enables us to infer a temporal restriction of growth, as well as cortical drift towards the posterior region of the element. Additionally, the identification of EFS in the pericortical region of the whole section, clearly suggests a decreased rate of growth (Fig 11B).

The first left phalange (GEOUACH.HS.PFI.1; Fig 11C) provides evidence of a relatively uniform growth around the cortex, and the maintenance of a homogeneous structure throughout the bone element. LB with a high degree of vascularization was also present surrounding the medullary cavity. Additionally, in the intracortical region FLB deposition was identified indicating rapid growth of the cortex, followed by the development of an EFS, thus suggesting a slow rate of growth (Fig 11C).

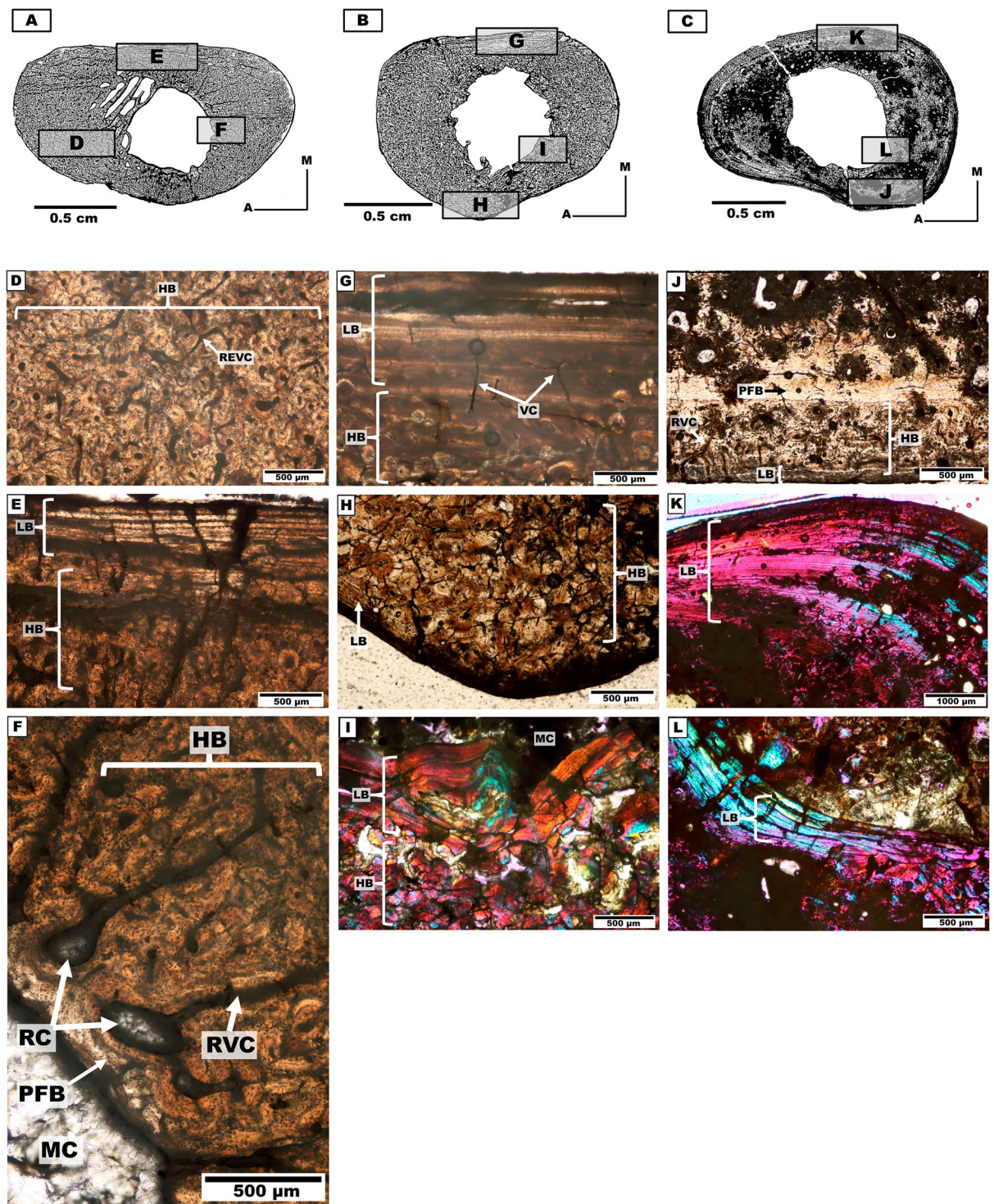


Fig 9. Tibia cross-sections of the mesotheriine notoungulate *Caraguatypotherium munozii* from the middle Miocene of Caragua, Huaylas formation. (A) Tibia cross-section for individual 4 (GEOUACH.HS.TI.1); (B) Tibia cross-section for individual 5 (GEOUACH.HS.TI.2); (C) Tibia cross section for individual 6 (GEOUACH.HS.TI.3); (D) HB in the intracortical region and presence of RVC (GEOUACH.HS.TI.1); (E) LB in the pericortical region and HB in the intracortical region (GEOUACH.HS.TI.1); (F) PFB in the endocortical region and RC (GEOUACH.HS.TI.1); (G) LB in the pericortical region, presence of VC and HB in the intracortical region (GEOUACH.HS.TI.2); (H) HB in the intracortical region; LB in the pericortical region (GEOUACH.HS.TI.2); (I) LB in the endocortical region and HB in the endocortical region (GEOUACH.HS.TI.2); (J) LB in the pericortical region, PFB in the interstitial spaces in the endocortical region (GEOUACH.HS.TI.3); (K) LB in the pericortical region and intracortical region (GEOUACH.HS.TI.3); (L) LB in the endocortical region (GEOUACH.HS.TI.3). For abbreviations refer to Fig 4.

<https://doi.org/10.1371/journal.pone.0273127.g009>

Table 2. Histological structures identified in previous studies where notoungulate remains were used.

Bone microstructure	<i>Nesodon tawereus</i> (Toxodontidae), MHNMRP-PV 1010 and MHNMRP-PV 1008 [36]	<i>Prototylotherium</i> sp. (Interatheriidae), YM-PU15241 and YM-PU15825 [18]	<i>Plesiotylotherium achirensis</i> (Mesotheriidae), MNNHN.F.ACH 18; MNNHN.F. ACH 34 and MNNHN.F.ACH 46 [18]	<i>Mesotherium</i> sp. (Mesotheriidae), (Pencil number: 273, ink label: 1938–583, Anat. Comp. 1878) [31]	<i>Toxodon</i> sp. ("Toxodontidae) (Link label: Anat. Comp. 1878) [31]	<i>Toxodon</i> sp. ("Toxodontidae), CTES-PZ 1564 and CTES-PZ 1595 [34]	<i>Paedotherium bonaerense</i> (Hegetotheriidae), MD-FM-13-44 [35]	<i>Thomashuxleya externa</i> (Isotemnidae), MPEF-PV 8166 [37]
Ulna		Ulna	Humerus	Femur	Humerus	Femur	Ulna	Ribs
Compact bone	X	X	X	X	X	X	X	X
Compacted coarse cancellous bone	X						X	X
Woven bone								X
Parallel fibered bone	X							
Lamellar bone	X							X
Osteocyte lagoons	X						X	
Vascular canal	X					X	X	X
Primary osteon					X		X	
Haversian system	X				X	X	X	X

<https://doi.org/10.1371/journal.pone.0273127.t002>

Table 3. Histological structures in the appendicular skeleton of *Caraguatypotherium munozii*. Abbreviations in Fig 4.

Appendicular skeleton/Histological structures	CCCB	FLB	PFB	LB	LTB	HB	VC	RVC	REVC	PVC	SO	PO
Humerus	X	X	X	X		X	X	X	X		X	X
Ulna	X	X	X	X			X	X	X	X	X	X
Metacarpal III		X	X	X			X				X	X
1 st Phalanges	X	X	X	X				X				
Femur	X		X	X	X	X		X			X	
Tibia			X	X	X		X	X	X			
Metatarsal II			X		X		X		X			X

<https://doi.org/10.1371/journal.pone.0273127.t003>

The humerus presents less deposition of PFB and LB in the pericortical region as compared with the more distal elements, indicating that this bone may have reached skeletal maturity later than the more distal elements, and therefore growing for a longer period of time during life. Nevertheless, bone remodelling appears more extensive in the cortex of the humerus samples in comparison to the more distal elements (metacarpal and phalange), which are scarcely remodelled. Thus, we infer that bone remodelling is present in more proximal elements of the forelimb (humerus). Overall, the forelimb bones of the individual 1 exhibited relatively mature bone histology evidenced by deposition of EFS in pericortical regions, which suggests slow somatic growth rates at the time of death.

Individual 2 (HUAY15-200). The histological structures of the right humerus (GEOUACH.HS.HD.1; Fig 11D) provided evidence supporting that the anterior side of the bone was under active growing at the time of death based on the presence of tissue with high rate of bone deposition and high degree of vascularisation.

The posterior side of the humeral section showed preservation of the humeral anatomy based on the presence of LB and PFB, a large area of the cortex allowing the retention of the elliptical shape of the element.

The lateral and medial sides presents similar histological structures characterised by having an intracortical region of FLB, exhibiting towards the posterior side LB. Based on this information, it can be inferred that the ontogenetic growth of the humerus would correspond with faster and constant growth in the anterior side (near the dectopectoral crest) contrasting with the slow growing tissues present towards the lateral, medial and posterior sides (Fig 11D).

The growth pattern of the ulna (GEOUACH.HS.UD.1; Fig 11E) is characterised by a deposit of fast-growing tissues in the anterior and posterior sides of the section, contrasting with the presence of low-growing tissue in the lateral and medial sides. This is in agreement with the shape of the analysed section, where higher length to width rate predominates (Fig 11E).

The histological features of the sample, corresponding to the first right phalange (GEOUACH.HS.PFD.1; Fig 11F), allow the identification of FLB and EFS in the pericortical region of the sample. The specimens also shows a high degree of vascularisation with VC opened to the cortical layer. The posterolateral side of the section shows cortical drift characterised by resorption from the medullary cavity and the deposition of periosteal LB to the lateral side of the section (Fig 11F).

The forelimb bones of the individual 2, shows predominance of FLB in intracortical regions, with some deposition of EFS in pericortical region. Additionally, all the samples presents high degree of vascularisation with VC opened to the cortical layer. According ly, the presence of EFS indicates that the individual has reached their somatic maturity (Fig 11D–11F).

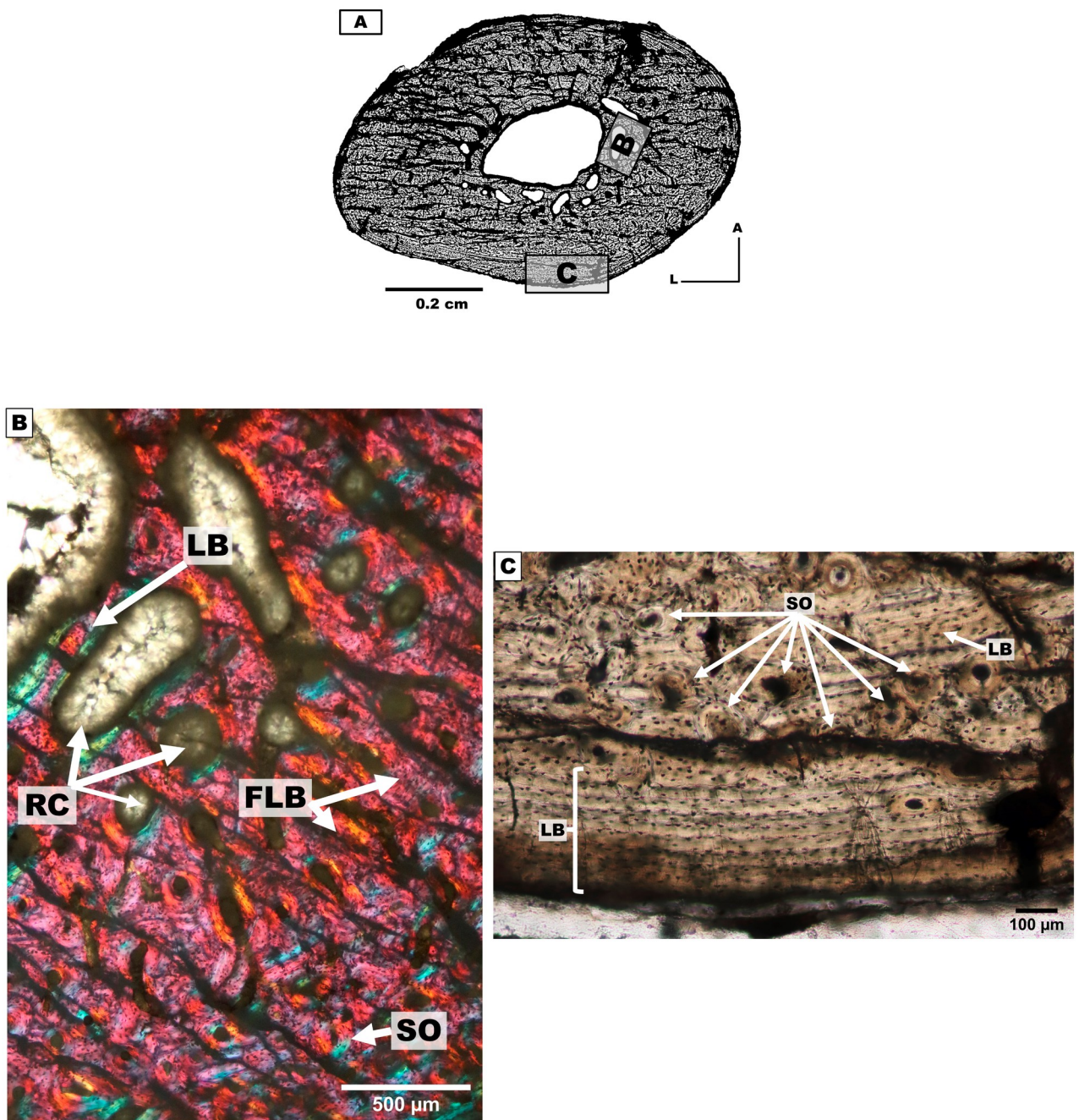


Fig 10. Metatarsal II cross-sections of the mesotheriine notoungulate *Caraguatypotherium munozi* from the middle Miocene of Caragua, Huaylas formation. (A) Metatarsal cross-section for individual 4 (GEOUACH.HS. MTSI.1); (B) RC and LB in the endocortical region, presence of SO in the endocortical region and FLB in the interstices (GEOUACH.HS. MTSI.1); (C) LB in the pericortical region, SO in the intracortical region (GEOUACH.HS. MTSI.1). For abbreviations refer to Fig 4.

<https://doi.org/10.1371/journal.pone.0273127.g010>

Individual 3 (HUAY17-05). The left humerus sample (GEOUACH.HS.HI.2; Fig 11G) from individual 3 corresponds to the smallest in size of the other two humeri analysed in this study (GEOUACH.HS.HI.1; and GEOUACH.HS.HD.1). The cortex is characterised by the presence of CCCB. In the anterolateral, lateral and posterior sides of the section, FLB is observed in smaller quantities than the CCCB. The presence of EFS in the humerus section

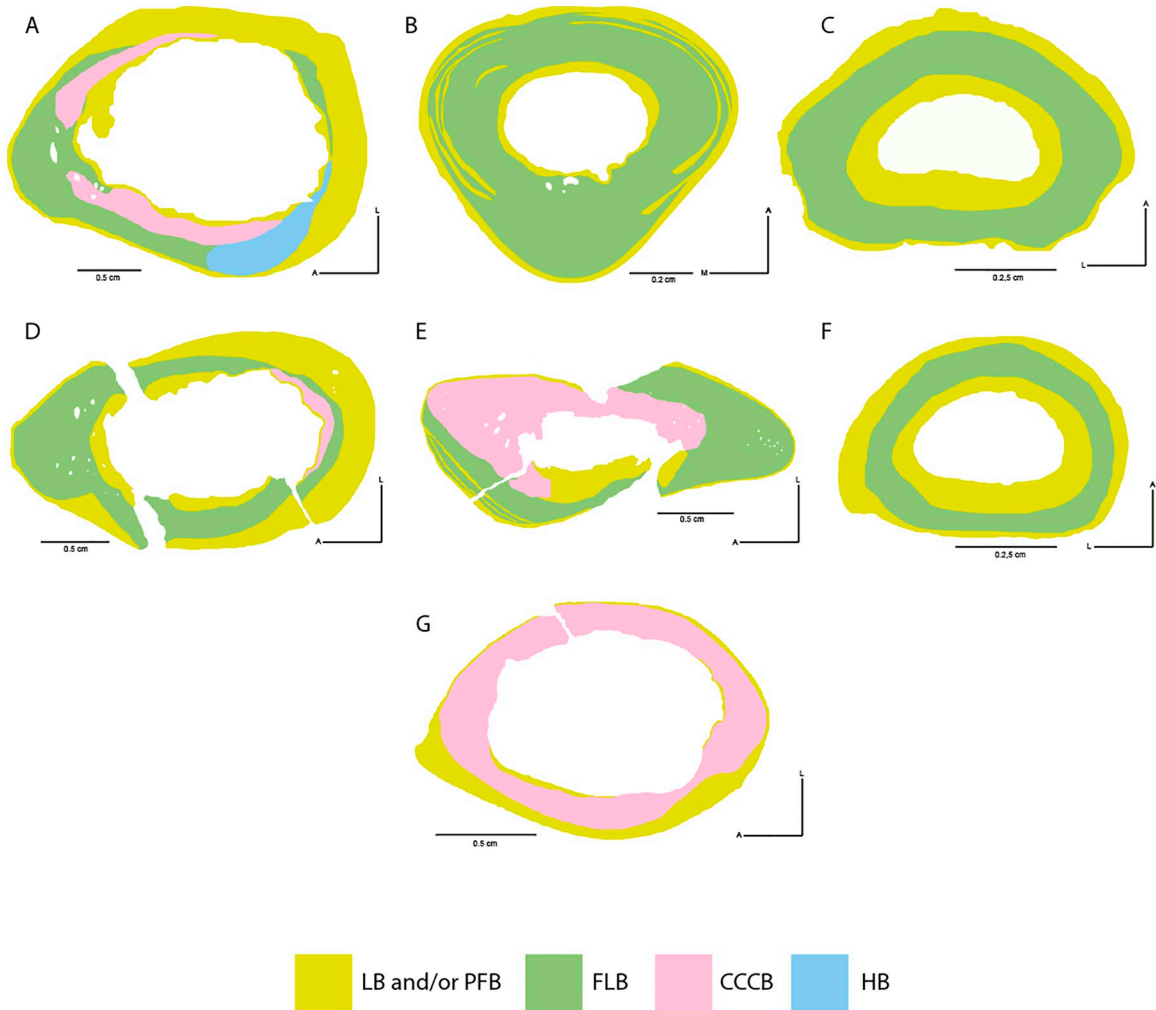


Fig 11. Types of bone tissue in section of *Caraguatypotherium munozi* from the middle Miocene of Caragua, Huaylas formation. Individual 1 (HUAY15-100): A, B and C, Individual 2 (HUAY 15-200): D, E and F, Individual 3 (HUAY17-05): G. (A) Left humerus (GEOUACH.HS.HI.1); (B) Left Metacarpal III (GEOUACH.HS.MTC.1); (C) 1st left phalange (GEOUACH.HS.PFI.1); (D) Right humerus (GEOUACH.HS.HD.1); (E) Right ulna (GEOUACH.HS.UD.1); (F) 1st left phalange (GEOUACH.HS.PFD.1); (G) Left humerus (GEOUACH.HS.HI.2). For abbreviations refer to Fig 4.

<https://doi.org/10.1371/journal.pone.0273127.g011>

shows that the individual had reached a state of somatic maturity, although other areas were still in the process of bone modelling (Fig 11G).

Individual 4 (HUAY16-100). The analysed bone elements from individual 4 correspond to appendicular elements of the left hindlimb. The sample of the left tibia (GEOUACH.HS.TI.1; Fig 12A) shows signs of remodelling in nearly the entire section. We identified a primary matrix corresponding to alternating bands of LB and PFB bone in the lateral side and formation of EFS. The trabecular bone in the medullary cavity indicates predomination of bone resorption (and cortical drift) towards the anterior side (Fig 12A).

In the metatarsal II (GEOUACH.HS.MTSI.1, Fig 12B), EFS is identified in the entire pericortical region maintaining similar thickness throughout the section. In the intracortical region, it is possible to observe FLB with resorption cavities in the endocortical region.

Overall, the hindlimb bones of the individual 4 show EFS, and no apparent active osteogenesis. The tibia exhibited showed considerably more remodelling than the metatarsal II (Fig 12A and 12B).

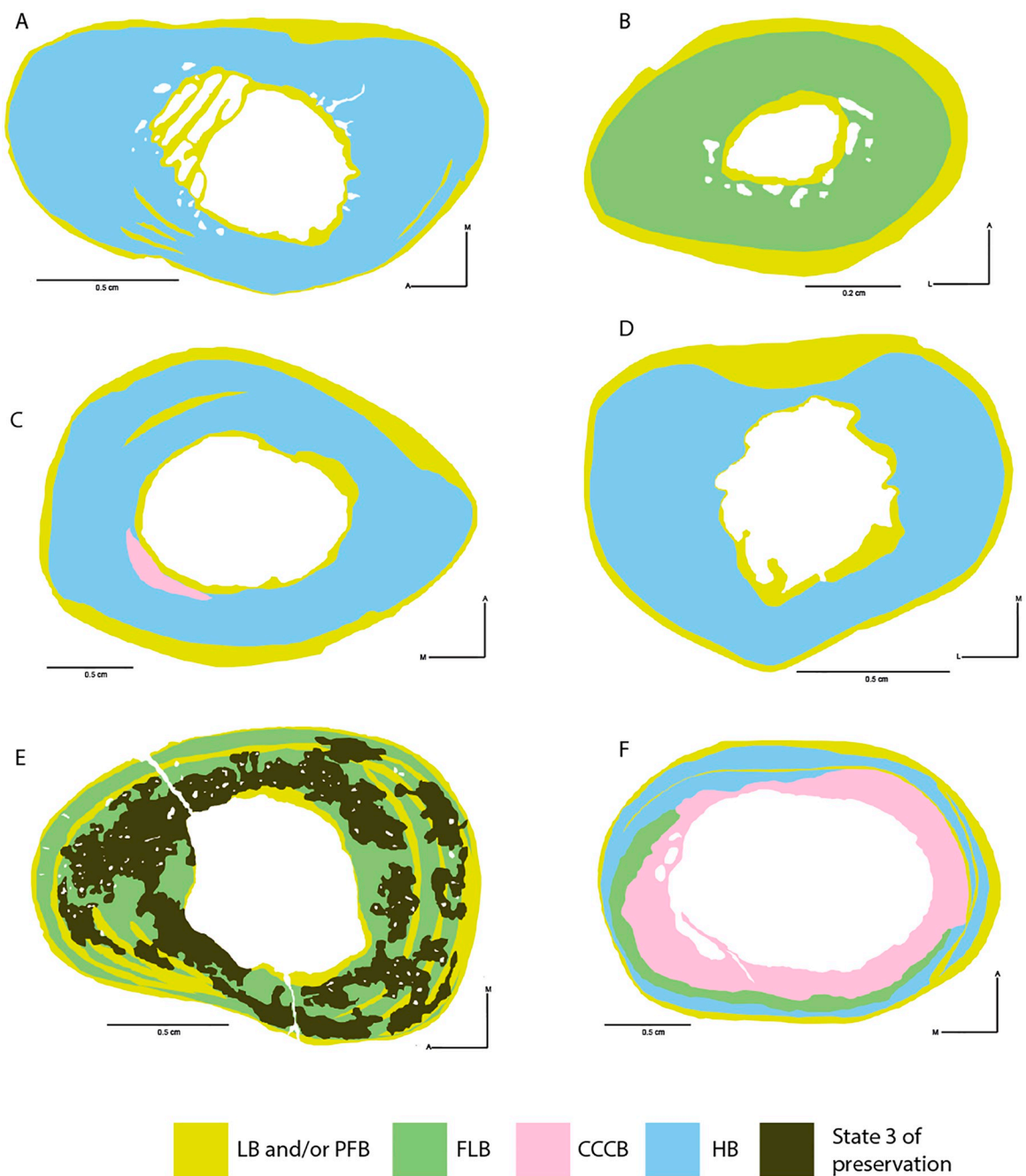


Fig 12. Types of bone tissue in section of *Caraguatypotherium munozi* from the middle Miocene of Caragua, Huaylas formation. Individual 4 (HUAY16-100): A and B, Individual 5 (HUAY15-84): C and D, Individual 6 (HUAY15-027): E, Individual 7 (HUAY17-02): F. (A) Left tibia (GEOUACH.HS.TI.1); (B) Left metatarsal II (GEOUACH.HS.MTSI.1); (C) Left femur (GEOUACH.HS.FI.2); (D) Left tibia (GEOUACH.HS.TI.1); (E) Left tibia (GEOUACH.HS.TI.3); (F) Right femur (GEOUACH.HS.FD.1). For abbreviations refer to Fig 4.

<https://doi.org/10.1371/journal.pone.0273127.g012>

Individual 5 (HUAY15-084). The tibia (GEOUACH.HS.TI.2, Fig 12C) and femur (GEOUACH.HS.FI.2, Fig 12D) of individual 5 showed a high degree of bone remodelling, although pericortical margins showed clear development of EFS. The anterior aspect of the femur showed zonal bone with intercalations of LB, suggesting a slowly and cyclical bone growth at the time of death. The tibia shows comparatively more remodelling than the femur,

and the EFS appears wider in the medial side and narrower in the lateral side compared to the rest of the section (Fig 12D).

It can be concluded that these bone elements have reached an advanced stage of development where the rate of bone deposition is low, with inactive periosteal surfaces and a high degree of bone remodelling throughout the cortex.

Individual 6 (HUAY15-027). Considering the intermediate and poor degree of preservation (state 2 and 3) of the tibia (GEOUACH.HS.TI.3, Fig 12E), it was possible to identify a pericortical region presenting EFS, which is represented by a thicker and more notorious band in the medial region. Relatively fast growing tissues were observed in the lateral, anterior and posterior regions, as well as presence of vascular canals opening towards the external surface of the bone (Fig 12E). Some patches of primary bone tissue (FLB) were identified in the intracortical region. These observations allow us to infer that this individual was still in an active stage of bone formation at the time of death.

Individual 7 (HUAY17-02). The femur (GEOUACH.HS.FD.1, Fig 12F) presents a histology characterised by proportional growth (similar thicknesses) in all regions of the bone cortex, and the presence of FLB in the intracortical region. An EFS is observed around the entire pericortical region.

Between the intracortical and pericortical regions, zonal bone with intercalations of LB were observed, which suggested that this bone was deposited slowly and cyclically (Fig 12F). Accordingly, we conclude that at the time of death, the femur was in an advanced stage of somatic maturity.

Humeral growth

Through the comparison of the three analysed humeri from specimens 1 to 3, it was possible to determine the ontogenetic growth of *C. munozi*. Thus, the humeral growth in this animal has been divided in two ontogenetic stages (Fig 11A, 11D and 11G).

1. A subadult stage corresponds to a specimen presenting a humerus with fused epiphyses. This stage is characterised by the absence of lamellar bone in the entire endocortical region. In the intracortical region there is a predominance of CCCB, characteristic of bone elements with a low degree of resorption, as well as FLB with VREC. The pericortical region presents a predominance of EFS, which is observed as a thin band only in the anteromedial, medial and posteromedial areas. In addition, there are radial vascular channels that open to the outside. This is shown in GEOUACH.HS.HI.2 (Fig 11G).
2. An adult ontogenetic stage corresponds to a specimen whose humerus presents fused epiphysis. With LB in the endocortical region covering the borders of the medullary cavity. The intracortical region is characterised by the predominance of the cortex with FLB and CCCB. In the pericortical region, EFS is present and it is thicker in the posterior area. These structures may be accompanied by reticular vascular canals opening to the exterior in some cases. This ontogenetic stage is shown in GEOUACH.HS.HI1 from individual 1 and GEOUACH.HS.HD1 from individual 2 (Fig 11A and 11D respectively).

Discussion

Ontogenetic reconstructions of mammalian species based on paleohistological assessments are scarce, principally due to the usually limited number of individuals available for this kind of analysis. This is particularly pronounced for the order Notoungulata, from which only brief descriptions of their bone microstructure have been reported [18, 28, 31–37] (Table 2).

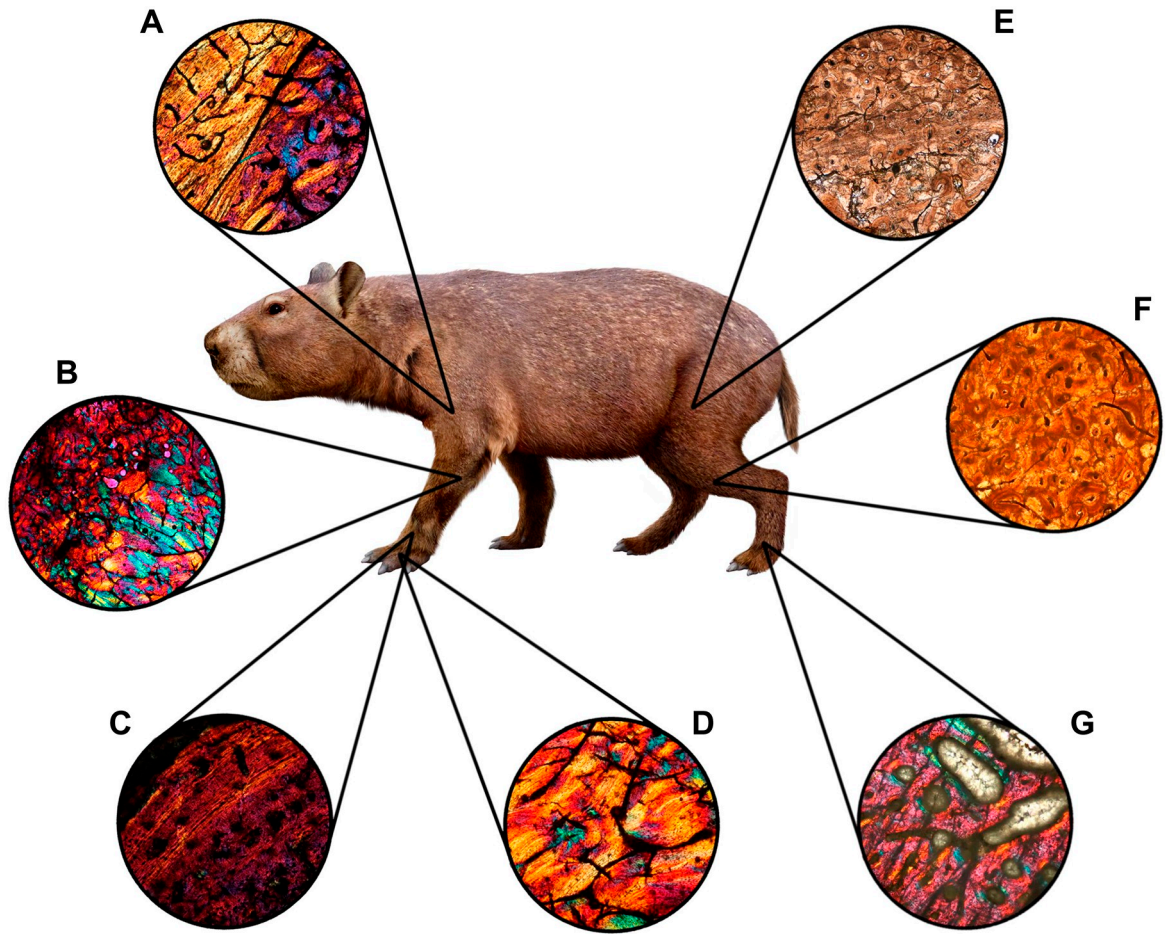


Fig 13. Reconstruction in life of *Caraguatypotherium munozi* from the middle Miocene of Caragua, Huaylas formation and histological detail. (A) Humerus; (B) Ulna; (C) Metacarpal III; (D) 1st Phalange; (E) Femur; (F) Tibia; (G) Metatarsal II. (Illustration made by Carlos Andres Espinosa Bustos).

<https://doi.org/10.1371/journal.pone.0273127.g013>

In this study, we evidenced the highly diverse bone microstructure of *C. munozi* (Table 3, Fig 13). The distribution and amount of bone tissues within the cortex showed high variation between different appendicular elements and even within the same bone, as well as during ontogeny. This indicates that the development of the long bones of *C. munozi* involves a complex process of bone modelling and remodelling, but also that bone elements within the same individual and sections growth at different rates. In general, our results confirm the presence of some bone tissues reported previously for mesotheriids [18, 31, 35], and present several previously undocumented tissue types to this group, thus suggesting that the histodiversity of mesotheriids is as rich as that of other extant mammals (e.g. [64, 65, 68, 74, 76, 77]).

Kolb et al. [28] made a preliminary “characterisation” of the paleohistology of Notoungulata, which have been described as presenting bones with a compacted, well vascularised cortex and mostly longitudinal vascular canals. Additionally, histological features in Notoungulata include the presence of few canals of regular orientation, large and abundant osteocyte lacunae, along with the identification of HB in the toxodontids *Toxodon* and *Nesodon*, as well as the mesotheriid *Mesotherium*. Surrounding the primary matrix, a tissue composed of LB and PFB bone is described, along with localised areas of woven bone characterised by rounded

osteocyte lacunae; and an outer cortex layer composed of PFB with few SO in clear contrast to the highly remodelled inner cortex [26].

For mesotheriids, the presence of HB [31], and PO and SO have only been previously described for *Mesotherium* sp. [18, 31]. Therefore, our investigation provides novel information for this group based on the histological variability of *C. munozi* (Table 3).

Thus, we reported for the first time in Mesotheriidae the presence of five different bone types: FLB, PFB, LB, HB, and CCCB [70, 71, 78, 79]. In addition to the description of vascularisation in previous studies (e.g. [28, 31, 34, 36, 37]), we include the presence of radial and reticular vascularisation, together with the plexiform orientation of the vascular canals.

The comparison between specimens used in this study and those of other notoungulates (lacking ontogenetic series) allowed us to have a better picture of the histological variability of the appendicular skeleton.

Interestingly, the presence of CCCB tissue, initially described by Enlow [70], has rarely been described in histological studies of fossil and extant mammals. The presence of this bone tissue has been described for young individuals [79], but in the case of the fossil remains from *C. munozi*, it is possible to find this type of tissue associated with EFS (Figs 11 and 12). Accordingly, it is inferred that CCCB remains in advanced ontogenetic stages of the animal. This process has also been observed in adult subterranean rodents (*Bathyergus suillus*: [68]) and adult aakvarks (*Orycteropus afer* [80]). Therefore, this tissue type is not exclusive to early ontogenetic stages, and the presence of this tissue in adulthood in *C. munozi* represents a remnant of the earlier endochondral bone formation and secondary compaction which was not obliterated during ontogeny, probably because a low bone resorption to maintain high levels of cortical thickening [68]. This would also suggest that the robust limb bones of *C. munozi* and other mesotheres that exhibit thick cortical walls in their long bones, might be adapted to increase the bending and torsional resistance experienced during activities of high impact, such as parasagittal scratch-digging (e.g. [68]). In this regard, some studies have suggested a certain degree of fossoriality in mesotheres [9].

Based on the results obtained, it is possible to support a significant size and histological variation of the forelimbs among sub-adult and adult individuals of *C. munozi*. This is important, especially considering that there is a strong size variation of individuals within close age ranges, that could lead to material identification to earlier ontogenetic stages based on macro-anatomic observations [42, 81, 82].

Additionally, our findings support that bone corresponding to younger stages of ontogenetic development in *C. munozi* present a structure that has already been described in other vertebrates [28, 67, 68, 80, 83]. This structure features a higher proportion of fast-growing microstructural bone elements in comparison with more advanced ontogenetic stages where slow-deposition of histological elements predominates.

Different studies have provided insights regarding the appendicular skeleton in mammals, pointing out that the best bone elements to be analysed are the tibia and femur, mainly because these elements exhibit low resorption and bone remodelling, so that the bone tissues developed early in ontogeny can still be observed [22, 30]. In contrast, we found that femur and tibia samples of *C. munozi* present high levels of bone remodelling in the entire cortex, indicating that these elements are not very informative for reconstructing the ontogeny of the animal.

Although in the present study is not possible to precise whether the hindlimbs of *C. munozi* reached skeletal maturity before the forelimbs (because the lack of hindlimbs and forelimbs of the same individual), our sample shows clearly a considerable difference growth patterns and microstructural arrangement between limbs, thus indicating a noticeable modular growth of the extremities. Such hypothesis should be tested using a larger and more complete dataset including individuals with both forelimbs and hindlimbs.

The *C. munozi* femur presents a stratified LB in the intracortical region. This marked stratification indicates a cessation and resumption of bone deposition in the bone element and may indicate a pause in the growth or even seasonality [21]. Similar growth interruption conformed by LB deposited in the intracortical region have also been described in fossil perissodactyls such as the equid *Hipparrisonini Hipparrison concudense*, probably indicating a cessation and a new resumption of growth in the animal [27]. It is not fully understood how exogenous and endogenous factors can influence the formation of this type of bone deposition. However, early and recent studies of extant taxa documenting cyclical growth in mammals have provided conclusive evidence that such variation in growth patterns are more widespread among mammals as previously thought. Köhler et al. [23] suggested that cyclical bone growth in mammals is a universal trait of homoeothermic endotherms and that the arrested growth observed during unfavourable seasons in endotherms may arise as part of a plesiomorphic thermo-metabolic strategy for energy conservation. The finding of growth marks and therefore cyclical growth in bone tissues of subterranean animals, such as African mole-rats (Bathyergidae) [68], the greater mole rat (Spalacidae) [84, 85] and moles (Talpidae) [86], which experience considerably lower levels of seasonality and environmental stress as compared to aboveground mammals supports this hypothesis, and suggests that environmental factors alone are not the only factor behind the process of cyclical growth. The finding of growth marks and cyclical bone growth in organisms from captive conditions such as naked mole-rats [64] and small primates [67], which experience lower levels of stress due to unlimited resources also support this hypothesis.

As previously described for other extinct animals [22, 28, 78, 79], the presence of ZB in *C. munozi* may represent the acquisition of a similar growth pattern in these extinct South American mammals, most likely evolved before the split from the rest of the mammalian lineages. Our analysis provides conclusive evidence for a highly complex pattern of bone modelling and remodelling in this taxon. It is important to mention that despite these growth patterns represent an endogenous aspect of the biology of mammals, other external factors such as environmental fluctuations and/or availability of food resources may also reinforce and/or be synchronized with growth. In this sense, increments of the rainfall patterns between 11–10 Ma have been recently interpreted from the stratigraphic record of Caragua and nearby localities [48, 53, 87–90]. This information suggests the onset of wetter conditions and ecosystem re-organization at the local and regional scales. A brief tectonic deformational pulse in the Pre-cordillera and concomitant uplift of the Western Andean orogenic front has also been recorded during this lapse [48, 51, 53, 88, 89]. Causality between both factors has been invoked through observed changes along the stratigraphic sections, including base level re-accommodation, modifications in the sedimentary regimes and watershed architecture, increment in basement-derived components, and associated landscape incision, beginning around 12 Ma [48, 53, 91]. Rapid climatic changes can lead to marked seasonality [90] imposing long lasting stressors over species and/or faunal interactions, with possible ecological and physiologic effects on individuals that can be observed in their skeletal structures, such as malnutrition or fibrous osteodystrophy [92, 93]. Similar factors also may impact populations, including the disruption of trophic dynamics, negative density-dependent effects, or selective local extirpation/extinctions [94]. Further research is required addressing the ontogeny and physiology of *C. munozi* and the remaining faunal components of Caragua, to assess how the environmental changes could be reflected in its histological record.

On the other hand, taxonomic limitations could sustain an alternative explanation for the observed differences. During the early to late Miocene diverse localities in Chile and nearby Bolivia such as Chucal, Cerdas, Nazareno, Quebrada Honda and Achiri, documents the sympatric coexistence is documented of more than one (two to three) mesotheriine species [39,

[95–99]. Body size differences between some of these species have been recognized, supporting generic-level taxonomic distinction (i.e., [97]). An underestimated interspecific diversity in Caragua's mesothere assemblage cannot be ruled out completely, especially concerning some of the isolated postcranial remains. Although different studies suggest that interspecific variation in some mesotherids is greater than previously thought [38, 33], intraspecific differences tend to be considered as intergeneric or interspecific differences as has been previously discussed (i.e. [42, 82, 98]). Despite this, morphological conservatism between the Caragua's samples and spatial proximity of the recovered individuals supports intraspecific ontogenetic disparity as the most plausible cause for such body size differences. New collections and detailed analysis of the morphological variability (and its histological correlation) within *Caraguatypotherium munozii* and other Miocene mesotheres are needed in order to understand the evolutionary ecology of mid-latitude faunas and its relationship with the proposed rapid environmental and climatic changes occurred in the Central Andes, as well as in the whole continent, during the Neogene. Future studies in this direction will reveal higher complexity in the Notoungulate fauna, which recent research (e.g. [11, 100]) such as the present one, are just starting to unveil.

Conclusions

Here we present the most comprehensive paleohistological study of Notoungulata, providing a detailed description of fore- and hindlimb of several individuals of the Mesotheriid *Caraguatypotherium munozii*, allowing a better understanding on the variety of histological structures shown by these animals. Results indicate high variability and growth of differences. In particular, humeri shows less bone resorption and remodelling favouring the study of ontogenetic stages, with all different bone types acquired throughout the life cycle of the animal. On the contrary, hindlimbs show excessive remodelling, erasing all early records. Based on these observations, the ontogenetic stage of individuals 4 to 7 (HUAY 16–100, HUAY 15–084, HUAY 15–027, HUAY 17–02) could not be determined, but they did reach somatic maturity on their hind limbs, which could be acquired in an early stage. Individuals 1 and 2 (HUAY15–100 and HUAY15–200) can be recognised as adults. Histological structures of bone deposition (high and low rates) are in agreement with proposed age ranges based on anatomical features (e.g. epiphyseal fusion). Although the humerus (GEOUACH.HI.2) of individual 3 (HUAY15–100) was expected to represent a juvenile or immature animal due to its small size (up to 40% smaller than the largest one) and external fibrous bones, instead it showed a slow rate of bone deposition indicating a cessation of growth, typical for a sub-adult or even an adult. The quantified low ontogenetic variability but higher size differences, suggests that exogenous factors could act as potential stressors associated with an unstable environment. This is supported by tectono-stratigraphic and isotopic evidence that shows rapid environmental and climatic changes during the beginning of the late Miocene associated with orogenic uplift and concomitant re-organization of the drainage systems along the western tectonic front of the Central Andes.

Supporting information

S1 Fig. Bone elements of individual 1 (HUAY15–100). A: Left humerus anterior view (GEOUACH.HS.HI.1); B: Left metacarpal anterior view (GEOUACH.HS.MTC.2); C: 3rd left phalange anterior view (GEOUACH.HS.TFI.1). Histological section area is indicated with a rectangle in black.
(TIFF)

S2 Fig. Bone elements of individual 2 (HUAY15-200). A: Right humerus posterior view (GEOUACH.HS.HD.1); B: Right ulna medial view (GEOUACH.HS.UD.1); C: Left femur anterior view (GEOUACH.HS.FI.1); D: 3rd right phalange anterior view (GEOUACH.HS.TFD.1). Histological section area is indicated with a rectangle in black. (TIFF)

S3 Fig. Bone element of individual 3 (HUAY17-05). A: Left humerus anterior view (GEOUACH.HS.HI.2). Histological section area is indicated with a rectangle in black. (TIFF)

S4 Fig. Bone elements of individual 4 (HUAY16-100). A: Left tibia anterior view (GEOUACH.HS.TI.1); B: Left metatarsal anterior view (GEOUACH.HS.MTSI.1). Histological section area is indicated with a rectangle in black. (TIFF)

S5 Fig. Bone elements of individual 5 (HUAY15-084). A: Left femur anterior view (GEOUACH.HS.FI.2); B: Left tibia anterior view (GEOUACH.HS.TI.2). Histological section area is indicated with a rectangle in black. (TIFF)

S6 Fig. A: Bone element of individual 6 (HUAY15-027). Left tibia anterior view (GEOUACH.HS.TI.3); B: Bone element of individual 7 (HUAY17-02), Right femur anterior view (GEOUACH.HS.FD.1). Histological section area is indicated with a rectangle in black. (TIFF)

Acknowledgments

This research was part of the master's thesis of JC-M (Campos-Medina, 2018), which was supervised by two of the authors KM, GM-S. We also acknowledge the suggestions and support of Drs. Ana Abarzúa and Carlos Figueroa during the completion of this master thesis. Special thanks are given to the Santos family and the community of Belén and Tignámar, for their support during the fieldwork and for giving access to the fossiliferous localities. We deeply thank the reviewers, particularly Dr. Fernández-Monescillo, which greatly improved the resulting manuscript. Prospecting and excavation authorizations were provided by the Consejo de Monumentos Nacionales (Council of National Monuments), Order no. 3362.

Author Contributions

Conceptualization: Jorge Campos-Medina, Germán Montoya-Sanhueza, Karen Moreno.

Formal analysis: Jorge Campos-Medina.

Investigation: Jorge Campos-Medina, Germán Montoya-Sanhueza.

Project administration: Karen Moreno.

Resources: Karen Moreno, Marcelo García.

Supervision: Germán Montoya-Sanhueza, Enrique Bostelmann Torrealba, Marcelo García.

Writing – original draft: Jorge Campos-Medina, Germán Montoya-Sanhueza, Karen Moreno.

Writing – review & editing: Jorge Campos-Medina, Germán Montoya-Sanhueza, Karen Moreno, Enrique Bostelmann Torrealba, Marcelo García.

References

1. Croft DA, Gelfo JN, López GM. Splendid Innovation: The Extinct South American Native Ungulates. *Annu Rev Earth Planet Sci.* 2020; 48: 259–290. <https://doi.org/10.1146/annurev-earth-072619-060126>
2. Chávez Hoffmeister MF. From Gondwana to the Great American Biotic Interchange: The Birth of South American Fauna. 2020. pp. 13–32. https://doi.org/10.1007/978-3-030-23918-3_2
3. Croft DA, López GM. Gondwanan Perspectives: Evolution, Biogeography, and Paleoecology of the Native Ungulates of South America. *Ameghiniana.* 2020; 57: 71–79. <https://doi.org/10.5710/AMGH.15.04.2020.3351>
4. Soria MF. Estudios sobre los Astrapotheria (Mammalia) del Paleoceno y Eoceno. *Ameghiniana.* 1987; 24: 21–34. Available: <http://www.ameghiniana.org.ar/index.php/ameghiniana/article/view/1897>
5. Ameghino F. Première contribution à la connaissance de la faune mammalogique des couches à Pyrotherium. *Bol del Inst Geográfico Argentino* 15. 1895; 1–60.
6. Ameghino F. Les mammifères crétacés de l'Argentine: deuxième contribution à la connaissance de la faune mammalogique des couches à Pyrotherium. *Bol Inst Geogr Argentino.* 1897; 18: 406–521.
7. Lydekker R. Contributions to a knowledge of the fossil vertebrates of Argentina, 3. A study of the extinct ungulates of Argentina. *Annales del Museo de La Plata* 2. 1983. <https://medium.com/@arifwicaksanaa/pengertian-use-case-a7e576e1b6bf>
8. Cifelli R. The phylogeny of the native South American ungulates. NY: Springer. In: Szalay F. S., Novacek M. J. M MC, editor. *Mammal Phylogeny.* NY: Springer. New York; 1993. pp. 195–216.
9. Shockley BJ, Flynn JJ. Morphological diversity in the postcranial skeleton of Casamayoran (? middle to late eocene) Notoungulata and foot posture in notoungulates. *Novitates American Museum.* 2007; 1–26.
10. Croft DA, Lorente M. No evidence for parallel evolution of cursorial limb adaptations among Neogene South American native ungulates (SANUs). *PLoS One.* 2021; 16: 5–10. <https://doi.org/10.1371/journal.pone.0256371> PMID: 34403434
11. Vera B, Medina-González P, Moreno K. Paleobiological inferences on middle Eocene native ungulates from South America: Functional morphological analysis of *Notostylops* and *Notopithecus*. *Journal of Morphology.* 2022; 283 (9): 1231–1256. <https://doi.org/10.1002/jmor.21499> PMID: 35915873
12. Buckley M. Ancient collagen reveals evolutionary history of the endemic South American “ungulates”. *Proc Biol Sci.* 2015; 282: 2014–2671. <https://doi.org/10.1098/rspb.2014.2671> PMID: 25833851
13. Welker F, Collins MJ, Thomas JA, Wadsley M, Brace S, Cappellini E, et al. Ancient proteins resolve the evolutionary history of Darwin's South American ungulates. *Nature.* 2015; 522: 81–84. <https://doi.org/10.1038/nature14249> PMID: 25799987
14. Westbury M, Baleka S, Barlow A, Hartmann S, Pajjmans JLA, Kramarz A, et al. A mitogenomic time-tree for Darwin's enigmatic South American mammal *Macrauchenia patachonica*. *Nat Commun.* 2017; 8. <https://doi.org/10.1038/ncomms15951> PMID: 28654082
15. Ameghino F. Recherches de morphologie phylogénétique sur les molaires supérieures des ongulés. *Annales del Museo Nacional de Buenos Aires. Serie 3a, Tomo III*, 1–541. Buenos Aires; 1904.
16. Cassini GH, Mendoza M, Vizcaíno SF, Bargo MS. Inferring habitat and feeding behaviour of early Miocene notoungulates from Patagonia. *Lethaia.* 2011; 44: 153–165. <https://doi.org/10.1111/j.1502-3931.2010.00231.x>
17. Cassini GH. Skull geometric morphometrics and paleoecology of santacrucian (late early miocene; Patagonia) native ungulates (astrapotheria, litopterna, and notoungulata). *Ameghiniana.* 2013; 50: 193–216. <https://doi.org/10.5710/AMGH.7.04.2013.606>
18. Houssaye A, Fernández V, Billet G. Hyperspecialization in some south american endemic ungulates revealed by long bone microstructure. *J Mamm Evol.* 2015; 23: 221–235. <https://doi.org/10.1007/s10914-015-9312-y>
19. Cassini GH, Flores DA, Vizcaíno SF. Postnatal ontogenetic scaling of Nesodontine (Notoungulata, Toxodontidae) cranial morphology. *Acta Zool.* 2012; 93: 249–259. <https://doi.org/10.1111/j.1463-6395.2011.00501.x>
20. Köhler M, Herridge V, Meneses CN, Fortuny J, Solé BM, Rosso A, et al. Palaeohistology reveals a slow pace of life for the dwarfed Sicilian elephant. *Sci Rep.* 2021; 11: 1–17. <https://doi.org/10.1038/s41598-021-02192-4> PMID: 34819557
21. Chinsamy-Turan A. The Microstructure of Dinosaur Bone. Deciphering Biology with Fine-Scale Techniques. Baltimore and London: The Johns Hopkins University Press.; 2005. 224 p. ISBN 0 8018 8120 X.
22. Köhler M, Moyà-Solà S. Physiological and life history strategies of a fossil large mammal in a resource-limited environment. *Proc Natl Acad Sci.* 2009; 106: 20354–20358. <https://doi.org/10.1073/pnas.0813385106> PMID: 19918076

23. Köhler M, Marin-Moratalla N, Jordana X, Aanes R. Seasonal bone growth and physiology in endotherms shed light on dinosaur physiology. *Nature*. 2012; 487: 358–361. <https://doi.org/10.1038/nature11264> PMID: 22763443
24. Padian K, Lamm E. Bone histology of fossil tetrapods. Advancing methods analysis, and interpretation. Berkeley, Los Angeles, London: University of California Press; 2013.
25. Kolb C, Scheyer TM, Lister AM, Azorit C, De Vos J, Schlingemann MAJ, et al. Growth in fossil and extant deer and implications for body size and life history evolution. *BMC Evol Biol*. 2015; 1–15. <https://doi.org/10.1186/s12862-015-0295-3> PMID: 25887855
26. Marín-Moratalla N, Jordana X, García-Martínez R, Köhler M. Tracing the evolution of fitness components in fossil bovids under different selective regimes. *Comptes Rendus—Palevol*. 2011; 10: 469–478. <https://doi.org/10.1016/j.crpv.2011.03.007>
27. Martínez-Maza C, Alberdi MT, Nieto-Díaz M, Prado JL. Life-history traits of the miocene *Hipparrison conudense* (Spain) inferred from bone histological structure. *PLoS One*. 2014; 9. <https://doi.org/10.1371/journal.pone.0103708> PMID: 25098950
28. Kolb C, Scheyer TM, Veitschegger K, Forasiepi AM, Amson E, Van der Geer AAE, et al. Mammalian bone paleohistology: a survey and new data with emphasis on island forms. *PeerJ*. 2015; 3: e1358. <https://doi.org/10.7717/peerj.1358> PMID: 26528418
29. Orlandi-Oliveras G, Jordana X, Moncunill-Solé B, Köhler M. Bone histology of the giant fossil dormouse *Hypnomys onicensis* (Gliroidae, Rodentia) from Balearic Islands. *Comptes Rendus—Palevol*. 2016; 15: 247–253. <https://doi.org/10.1016/j.crpv.2015.05.001>
30. García-Martínez R, Marín-Moratalla N, Jordana X, Köhler M. The ontogeny of bone growth in two species of dormice: Reconstructing life history traits. *Comptes Rendus—Palevol*. 2011; 10: 489–498. <https://doi.org/10.1016/j.crpv.2011.03.011>
31. de Ricqlès A, Taquet P, De Buffrenil V. “Rediscovery” of Paul Gervais’ paleohistological collection. *Geodiversitas*. 2009; 31: 943–971. <https://doi.org/10.5252/g2009n4a943>
32. Simpson G.G. 1940 The names Mesotherium and Typotherium. *American Journal of Science*. 238: 518–521.
33. Fernández-Monescillo M, Croft DA, Pujos F, Antoine PO Taxonomic history and intraspecific analysis of Mesotherium cristatum (Mammalia, Notoungulata, Mesotheriidae) from the Early-Middle Pleistocene of Buenos Aires Province, Argentina, *Historical Biology*, 2022 <https://doi.org/10.1080/08912963.2022.2074844>
34. Tomassini RL, Miño-Boilini ÁR, Zurita AE, Montalvo CI, Cesaretti N. Modificaciones fosildiagenéticas en *Toxodon platensis* Owen, 1837 (Notoungulata, Toxodontidae) del Pleistoceno tardío de la provincia de Corrientes, Argentina. *Rev Mex Ciencias Geológicas*. 2015; 32: 283–292.
35. Tomassini RL, Montalvo CI, Manera T, Visconti G. Mineralogy, geochemistry and paleohistology of pliocene mammals from the Monte Hermoso Formation (Argentina). *Paedotherium bonaerense* (Notoungulata, Hegetotheriidae) as a Case Study. *Ameghiniana*. 2014; 51: 385–395. <https://doi.org/10.5710/AMGH.01.07.2014.2737>
36. Forasiepi AM, Cerdeño E, Bond M, Schmidt GI, Naipauer M, Straehl FR, et al. New toxodontid (Notoungulata) from the Early Miocene of Mendoza, Argentina. *Palaontologische Zeitschrift*. 2014; 89: 611–634. <https://doi.org/10.1007/s12542-014-0233-5>
37. Carrillo JD, Asher RJ. An exceptionally well-preserved skeleton of *Thomashuxleya externa* (Mammalia, Notoungulata), from the Eocene of Patagonia, Argentina. *Palaeontol Electron*. 2017;20.2.34A: 1–33. <https://palaeo-electronica.org/content/2017/1930-anatomy-and-systematics-of-thomashuxleya-externa-notoungulata>
38. Francis JC. Los géneros de la subfamilia Mesotheriinae (Typotheria, Notoungulata) de la República Argentina. *Boletín del Laboratorio de Paleontología de Vertebrados*. 1965; 1: 7–31.
39. Villarroel C. Les Mesotherines (Notoungulata, Mammalia) du Pliocene de Bolivie. *Leurs Rapports Avec Ceux D’Argentine*. Ann Paleontol. 1974; 60: 245–281.
40. Billet G, De Muizon C, Mamani Quispe B. Late Oligocene mesotheriids (Mammalia, Notoungulata) from Salla and Lacayani (Bolivia): implications for basal mesotheriid phylogeny and distribution. *Zool J Linn Soc*. 2008; 152: 153–200. <https://doi.org/10.1111/j.1096-3642.2007.00388.x>
41. Shockley BJ, Billet G, Salas-Gismondi R. A new species of *Trachytherus* (Notoungulata: Mesotheriidae) from the late Oligocene (Deseadan) of Southern Peru and the middle latitude diversification of early diverging mesotheriids. *Zootaxa*. 2016 May 18; 4111(5):565–83. <https://doi.org/10.11646/zootaxa.4111.5.3> PMID: 27395103.
42. Cerdeño E, Vera B, Combina AM. A new early Miocene Mesotheriidae (Notoungulata) from the Mariño Formation (Argentina): Taxonomic and biostratigraphic implications. *J South Am Earth Sci*. 2018; 88: 118–131. <https://doi.org/10.1016/j.jsames.2018.06.016>

43. Armella MA and Ercoli D. An evaluation of the dental features used to distinguish *Typhotheriopsis* from *Pseudotyphotherium* (Mesotheriidae, Notoungulata): reappraisals and proposals regarding their systematic value. *Ameghiniana*. 2018; 55: 592–599.
44. Cione AL, Tonni E. Bioestratigrafía basada en mamíferos del Cenozoico superior de la región pampeana. In: *Geología y Recursos Minerales de la Provincia de Buenos Aires. Relatorio del XVI Congreso Geológico Argentino*. de Barrio R, Etcheverry RO, Caballé M, Llambías E. 2005.
45. Fernández-Monescillo M, Martínez G, García López D, Frechen M, Romero-Lebrón E, Krapovickas JM, et al. The last record of the last typhotherid (Notoungulata, Mesotheriidae, *Mesotherium cristatum*) for the middle Pleistocene of the western Pampean region, Córdoba Province, Argentina, and its biostratigraphic implications. *Quat Sci Rev*. 2023; 301: 107925. <https://doi.org/10.1016/j.quascirev.2022.107925>
46. Patterson B. Notas acerca del cráneo de un ejemplar juvenil de *Mesotherium cristatum*. *Revista del Museo Municipal de Ciencias Naturales y Tradicional de Mar de Plata*. 1952; 1: 71–78.
47. García GM, Gardeweg PM, Clavero RJ, Héral G, Hoja Arica, Región de Tarapacá, Escala 1:250.000. SERNAGEOMIN. 2004. p. 150.
48. García M, Riquelme R, Farías M, Héral G, Charrier R. Late Miocene-Holocene canyon incision in the western Altiplano, northern Chile: Tectonic or climatic forcing? *J Geol Soc London*. 2011; 168: 1047–1060. <https://doi.org/10.1144/0016-76492010-134>
49. García M, Héral G. Fault-related folding, drainage network evolution and valley incision during the Neogene in the Andean Precordillera of Northern Chile. *Geomorphology*. 2005; 65: 279–300. <https://doi.org/10.1016/j.geomorph.2004.09.007>
50. Muñoz N, Charrier R. Uplift of the western border of the Altiplano on a west-vergent thrust system, Northern Chile. *J South Am Earth Sci*. 1996; 9: 171–181. [https://doi.org/10.1016/0895-9811\(96\)00004-1](https://doi.org/10.1016/0895-9811(96)00004-1)
51. Charrier R, Héral G, Pinto L, García M, Riquelme R, Farías M, et al. Cenozoic tectonic evolution in the Central Andes in northern Chile and west central Bolivia: Implications for paleogeographic, magmatic and mountain building evolution. *Int J Earth Sci*. 2013; 102: 235–264. <https://doi.org/10.1007/s00531-012-0801-4>
52. Gradstein F, Ogg JG, Schmitz MD, Ogg GM. *Geologic Time Scale 2020*, Elsevier, Amsterdam. 2020; 2: 1390 pp.
53. Madella A, Delunel R, Akçar N, Schlunegger F, Christl M. 10Be-inferred paleo-denudation rates imply that the mid-Miocene western central Andes eroded as slowly as today. *Sci Rep*. 2018; 8: 1–10. <https://doi.org/10.1038/s41598-018-20681-x> PMID: 29396427
54. Bargo MS, Reguero MA. El primer registro de un mamífero fósil en el extremo septentrional de Chile. *Ameghiniana*. 1989; 26: 239.
55. Salinas P, Villarroel C, Marshall M, Sepulveda P, Muñoz. N. *Typhotheriopsis* sp. (Notoungulata, Mesotheriidae), mamífero del Mioceno Superior en las cercanías de Belén, Arica, Norte de Chile.pdf. VI Congr Geol Chil Resum Expand. 1991; 314–317.
56. Flynn JJ, Croft DA, Charrier R, Wyss AR, Héral G, García M. New Mesotheriidae (Mammalia, Notoungulata, Typhotheria), geochronology and tectonics of the Caragua area, northernmost Chile. *J South Am Earth Sci*. 2005; 19: 55–74. <https://doi.org/10.1016/j.jsames.2004.06.007>
57. Montoya-Sanhueza G, Moreno K, Bobe R, Carrano MT, García M, Corgne A. Peltekiliidae and Mesotheriidae (Mammalia) from late Miocene strata of Northern Chilean Andes, Caragua. *J South Am Earth Sci*. 2017; 75: 51–65. <https://doi.org/10.1016/j.jsames.2017.01.009>
58. Bostelmann E, Castro N, Moreno K, Fosdick J, Campos-Medina J, Croft DA, et al. Stratigraphy and paleontology of Caragua, Arica and Parinacota regions, Chile, part 2: biostratigraphy and geochronology of the late Miocene sedimentary sequence. *Actas del XV Congr Geológico Chil*. 2018.
59. Rasband, W.S., ImageJ, U. S. National Institutes of Health, Bethesda, Maryland, USA, <https://imagej.nih.gov/ij/>, 1997–2018.
60. Fernández-Monescillo M, Quispe BM, Pujos F, Antoine PO. Functional Anatomy of the Forelimb of *Plesiotypeotherium achirense* (Mammalia, Notoungulata, Mesotheriidae) and Evolutionary Insights at the Family Level. *J Mamm Evol*. 2018; 25: 197–211. <https://doi.org/10.1007/s10914-016-9372-7>
61. Reuil S, Muzzopappa P. 3D casts from natural molds: A case study in fossil frogs. *Publ Electron la Asoc Paleontol Argentina*. 2019; 19: 1–6. <https://doi.org/10.5710/PEAPA.14.04.2019.280>
62. Cerdeño E, Vera B, Schmidt GI, Pujos F, Quispe BM. An almost complete skeleton of a new Mesotheriidae (Notoungulata) from the Late Miocene of Casira, Bolivia. *J Syst Palaeontol*. 2012; 10: 341–360. <https://doi.org/10.1080/14772019.2011.569576>
63. Chinsamy A, Raath M a. Preparation of fossil bone for histological examination. *Palaeontol Africana*. 1992; 29: 39–44.

64. Montoya-Sanhueza G, Bennett NC, Oosthuizen MK, Dengler-Crish CM, Chinsamy A. Long bone histomorphogenesis of the naked mole-rat: Histodiversity and intraspecific variation. *J Anat.* 2020; 1–25. <https://doi.org/10.1111/joa.13381> PMID: 33305850
65. Montoya-Sanhueza G, Bennett NC, Oosthuizen MK, Dengler-Crish CM, Chinsamy A. Bone remodeling in the longest living rodent, the naked mole-rat: Interelement variation and the effects of reproduction. *J Anat.* 2021. <https://doi.org/10.1111/joa.13404> PMID: 33554344
66. Montoya-Sanhueza G, Šaffa G, Šumbera R, Chinsamy A, Jarvis JUM, Bennett NC. Fossorial adaptations in African mole-rats (Bathyergidae) and the unique appendicular phenotype of naked mole-rats. *Commun Biol.* 2022; 5: 1–14. <https://doi.org/10.1038/s42003-022-03480-z> PMID: 35650336
67. Castanet J, Croci S, Aujard F, Perret M, Cubo J, De Margerie E. Lines of arrested growth in bone and age estimation in a small primate: *Microcebus murinus*. *J Zool.* 2004; 263: 31–39. <https://doi.org/10.1017/S0952836904004844>
68. Montoya-Sanhueza G, Chinsamy A. Long bone histology of the subterranean rodent *Bathyergus suillus* (Bathyergidae): ontogenetic pattern of cortical bone thickening. *J Anat.* 2017; 230: 203–233. <https://doi.org/10.1111/joa.12547> PMID: 27682432
69. Hollund HI, Jans MME, Collins MJ, Kars H, Joosten I, Kars SM. What happened here? Bone histology as a tool in decoding the postmortem histories of archaeological bone from Castricum, The Netherlands. *Int J Osteoarchaeol.* 2012; 22: 537–548. <https://doi.org/10.1002/oa.1273>
70. Enlow DH. Principles of bone remodeling. *Am Lect Ser.* 1963; 85: 6991–7006.
71. Francillon-Vieillot H, de Buffrénil V, Castanet J, Géraudie J, Meunier FJ, Sire JY, et al. Microstructure and mineralization of vertebrate skeletal tissues. 1990. pp. 175–234. <https://doi.org/10.1029/SC005p0175>
72. de Ricqlès A, Meunier FJ, Castanet J. Comparative microstructure of bone. *Bone, Volume 3 Bone Matrix and Bone Specific Products.* Boca Raton: CRC Press; 1992. p. 333.
73. Chinsamy A, Hurum JH. Bone microstructure and growth patterns of early mammals. *Acta Palaeontol Pol.* 2006; 51: 325–338.
74. Warshaw J. Comparative primate bone microstructure: Records of life history, function, and phylogeny. *Vertebr Paleobiol Paleoanthropology.* 2008; 385–425. https://doi.org/10.1007/978-1-4419-6997-0_18
75. McFarlin SC, Terranova CJ, Zihlman AL, Bromage TG. Primary bone microanatomy records developmental aspects of life history in catarrhine primates. *J Hum Evol.* 2016; 92: 60–79. <https://doi.org/10.1016/j.jhevol.2015.12.004> PMID: 26989017
76. Straehl FR, Scheyer TM, Forasiepi AM, MacPhee RD, Sánchez-Villagra MR. Evolutionary patterns of bone histology and bone compactness in Xenarthran Mammal long bones. *PLoS One.* 2013; 8. <https://doi.org/10.1371/journal.pone.0069275> PMID: 23874932
77. Heck CT, Varricchio DJ, Gaudin TJ, Woodward HN, Horner JR. Ontogenetic changes in the long bone microstructure in the nine-banded armadillo (*Dasyurus novemcinctus*). *PLoS One.* 2019; 14: 1–24. <https://doi.org/10.1371/journal.pone.0215655> PMID: 31022247
78. Chinsamy-Turan A. The Microstructure of bones and teeth of nonmammalian therapsids. *Forerunners of Mammals.* Indiana University Press; 2012. pp. 65–90.
79. Hurum JH, Chinsamy-Turan A. The radiation, bone histology, and biology of early mammals. *Forerunners of Mammals.* Indiana University Press; 2012. pp. 249–270. <http://www.mediafire.com/?6b7ak67x7bc0p56>
80. Legendre LJ, Botha-Brink J. Digging the compromise: Investigating the link between limb bone histology and fossoriality in the aardvark (*Orycteropus afer*). *PeerJ.* 2018; 2018: 1–40. <https://doi.org/10.7717/peerj.5216> PMID: 30018860
81. Armella MA, Nasif NL, Cerdeño E. Small-sized mesotheriines (Mesotheriidae, Notoungulata) from Northwestern Argentina: Systematic, chronological, and paleobiogeographic implications. *J South Am Earth Sci.* 2018; 83: 14–26. <https://doi.org/10.1016/j.jsames.2018.02.002>
82. Cerdeño E, Schmidt GI. Milk molars or extra premolars in Mesotheriinae (Mesotheriidae, Notoungulata): New insights into an old controversy. *Geobios.* 2013; 46: 195–202. <https://doi.org/10.1016/j.geobios.2012.10.014>
83. Castanet J. Time recording in bone microstructures of endothermic animals; functional relationships. *Comptes Rendus—Palevol.* 2006; 5: 629–636. <https://doi.org/10.1016/j.crpv.2005.10.006>
84. Hamar MA. Prodanascu. Age determination in *Spalax microphthalmus* (Rodentia, Spalacidae). *Ann Zool Fennici.* 1971; 8: 60–63.
85. Puzachenko A. Age determination of *Spalax microphthalmus* (Rodentia, Spalacidae). *Zool Zhurnal.* 1991; 70: 113–124.

86. Klevezal GA. Recording structures of mammals. Determination of age and reconstruction of life history. Rotterdam: Recording Structures of Mammals: Determination of Age and Reconstruction of Life History. 1996.
87. Castro N, Bostelmann E, Moreno K, García M. Stratigraphy and paleontology of Caragua, Arica and Parinacota regions, Chile, part 1: lithostratigraphy and depositional environments of the late Miocene sedimentary sequence. *Actas del XV Congr Geológico Chil.* 2018.
88. Schlunegger F, Kober F, Zeilinger G, von Rotz R. Sedimentology-based reconstructions of paleoclimate changes in the Central Andes in response to the uplift of the Andes, Arica region between 19 and 21°S latitude, northern Chile. *Int J Earth Sci.* 2010; 99: 123–137. <https://doi.org/10.1007/s00531-010-0572-8>
89. Schlunegger F, Norton KP, Delunel R, Ehlers TA, Madella A. Late Miocene increase in precipitation in the Western Cordillera of the Andes between 18–19°S latitudes inferred from shifts in sedimentation patterns. *Earth Planet Sci Lett.* 2017; 462: 157–168. <https://doi.org/10.1016/j.epsl.2017.01.002>
90. Prámparo MB, Antoine PO, Marivaux L, Andrade Flores R, Fernández-Monescillo M, Boscaini A, et al. Occurrence of *Cyclusphaera scabrata* in Achiri (late middle-early late Miocene?, Bolivian Altiplano): Paleogeographical implication. *J South Am Earth Sci.* 2022; 119. <https://doi.org/10.1016/j.jsames.2022.103990>
91. Evenstar LA, Mather AE, Hartley AJ. Using spatial patterns of fluvial incision to constrain continental-scale uplift in the Andes. *Glob Planet Change.* 2020; 186: 103119. <https://doi.org/10.1016/j.gloplacha.2020.103119>
92. Rothschild BM, Martin LD. Paleopathology: disease in the fossil record. CRC Press. 1993.
93. Lyras GA, Giannakopoulou A, Lillis T, van der Geer AAE. Paradise lost: Evidence for a devastating metabolic bone disease in an insular Pleistocene deer. *Int J Paleopathol.* 2019; 24: 213–226. <https://doi.org/10.1016/j.ijpp.2018.12.003> PMID: 30572299
94. Patterson BR, Power VA. Contributions of forage competition, harvest, and climate fluctuation to changes in population growth of northern white-tailed deer. *Oecologia.* 2002; 130: 62–71. <https://doi.org/10.1007/s004420100783> PMID: 28547026
95. Villarroel C. Edades y correlaciones de algunas unidades litoestratigráficas del Altiplano Boliviano y estudio de algunos representantes mesoteriinos. *Rev la Acad Nac Ciencias Boliv.* 1978;1: 159–170.
96. Oiso Y. New land mammal locality of middle Miocene (Colloncuran) age from Nazareno, southern Bolivia, p. 653–672. Suárez-Soruco, R. (ed.), *Yacimientos Petrolíferos Fiscales Bolivianos, Santa Cruz.* In: Suárez-Soruco R, editor. *Fósiles y Facies de Bolivia.* 1991. pp. 653–672.
97. Croft DA. Notoungulata and Litopterna of the Early Miocene Chucal Fauna, Northern Chile. *Fieldiana Geol.* 2004; 1: 1–52. [https://doi.org/10.3158/0096-2651\(2004\)50\[1:nalote\]2.0.co;2](https://doi.org/10.3158/0096-2651(2004)50[1:nalote]2.0.co;2)
98. Croft DA. The middle Miocene (Laventan) Quebrada Honda Fauna, southern Bolivia and a description of its notoungulates. *Palaeontology.* 2007; 50: 277–303. <https://doi.org/10.1111/j.1475-4983.2006.00610.x>
99. Townsend B, Croft D a. Middle Miocene Mesotheriine diversity at Cerdas, Bolivia and a reconsideration of *Plesiotypotherium minus*. *Palaeontol Electron.* 2010; 13: 1A–36. Available: http://www.uv.es/pe/2010_1/192/192.pdf
100. Rodrigues HG, Cornette R, Clavel J, Cassini G, Bhullar BAS, Fernández-Monescillo M, et al. Differential influences of allometry, phylogeny and environment on the rostral shape diversity of extinct South American notoungulates. *R Soc Open Sci.* 2018; 5: 171816. <https://doi.org/10.1098/rsos.171816> PMID: 29410874